Solid-state emitting twisted π-conjugates as AIE-active DSE-gens: *In vitro* anticancer properties against FaDu and 4T1 with biocompatibility and bioimaging

Shouvik Bhuin,[a] Pravesh Sharma,[b] Purbali Chakraborty,[b] Onkar Kulkarni,[b] Manab Chakravarty[a]*

[a.] *Department of Chemistry, Birla Institute of Technology and Science-Pilani, Hyderabad Campus Jawahar Nagar, Shamirpet, Hyderabad, Telangana, 500078, India. E-mail: manab@hyderabad.bits-pilani.ac.in*

[b.] *Department of Pharmacy, Birla Institute of Technology and Science-Pilani, Hyderabad Campus Jawahar Nagar, Shamirpet, Hyderabad, Telangana, 500078, India.*

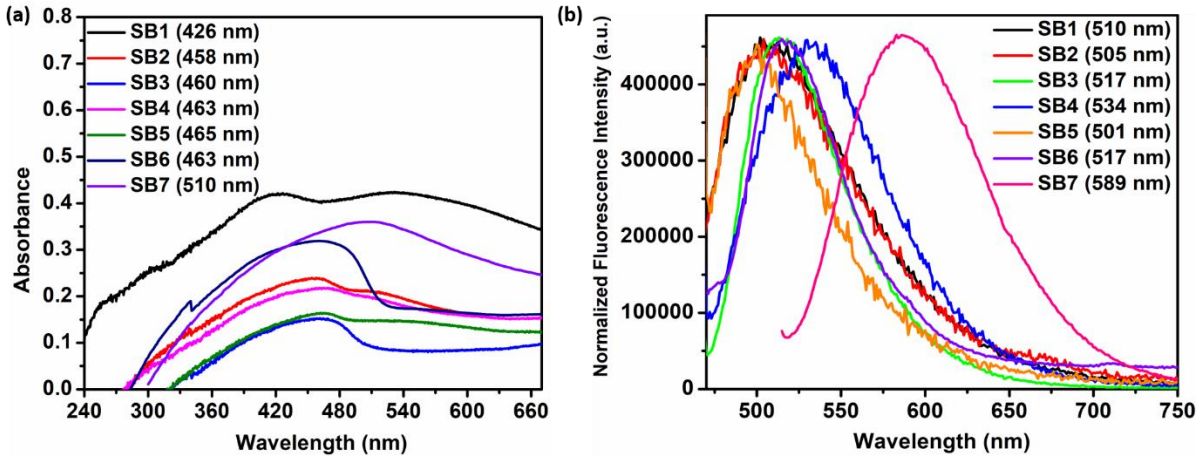

Fig. S1 Solid-state (a) absorbance and (b) emission of indole-anthracenyl derivatives

Table S1 Solid state fluorescence properties of the synthesized indole-linked anthracenyl π-conjugates

Compound	$\lambda_{abs\ max}$ (nm)	$\lambda_{em\ max}$ (nm)	$\phi_{f\ solid}$ (%)
SB1	426	510	7.04
SB2	458	505	1.29
SB3	460	517	26.64
SB4	463	534	10.28
SB5	465	501	7.00
SB6	463	517	20.11
SB7	510	589	2.66

The solid-state absolute quantum yield values were obtained with absolute errors within ~±2%

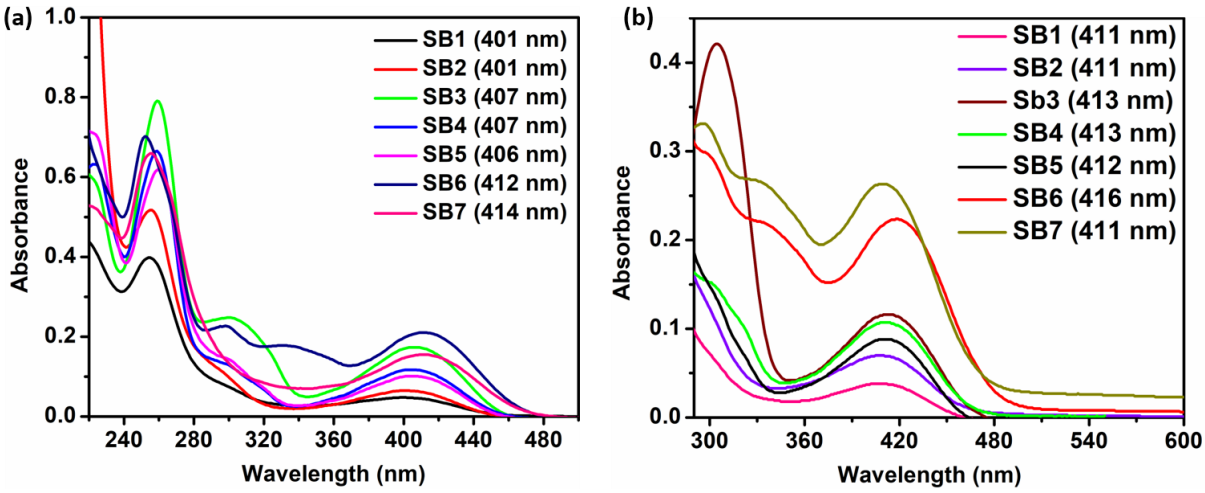

Fig. S2 (a) Absorbance in MeCN and (b) absorbance in DMSO of indole-anthracenyl derivatives (corresponding $\lambda_{max.abs.}$ have been mentioned)

Table S2 Steady-state photophysical parameters of DSEgens

Compound	Solvent	$\lambda_{max.abs}$ (nm)	$\lambda_{.em}$ (nm)	Stokes shift (nm) with respect to the $\lambda_{.em\ max}$	ϕ_f (%)
SB1	MeCN	401	427 (max), 450	26	1.63
SB2	MeCN	401	483	82	2.13
SB3	MeCN	407	493	86	2.54
SB4	**MeCN**	**407**	**427, 508 (max)**	**101**	**2.53**
SB5	MeCN	406	428, 507 (max)	101	3.19
SB6	MeCN	412	548	136	3.91
SB7	MeCN	414	457, 619 (max)	205	1.91
SB1	DMSO	411	436, 512 (max)	101	1.21
SB2	DMSO	411	503	92	1.53
SB3	DMSO	413	510	97	2.76
SB4	**DMSO**	**413**	**441, 520 (max)**	**107**	**2.18**
SB5	DMSO	412	517	105	2.10
SB6	DMSO	416	555	139	4.18
SB7	DMSO	411	531, 623 (max)	92	1.49

Some of these molecules have other shoulder peaks of emissions in a different region from the maxima. **SB3** in DMSO has a very broad spectrum covering from 427 nm to 720 nm almost with a max (maximum) at 510 nm without any shoulder emission.

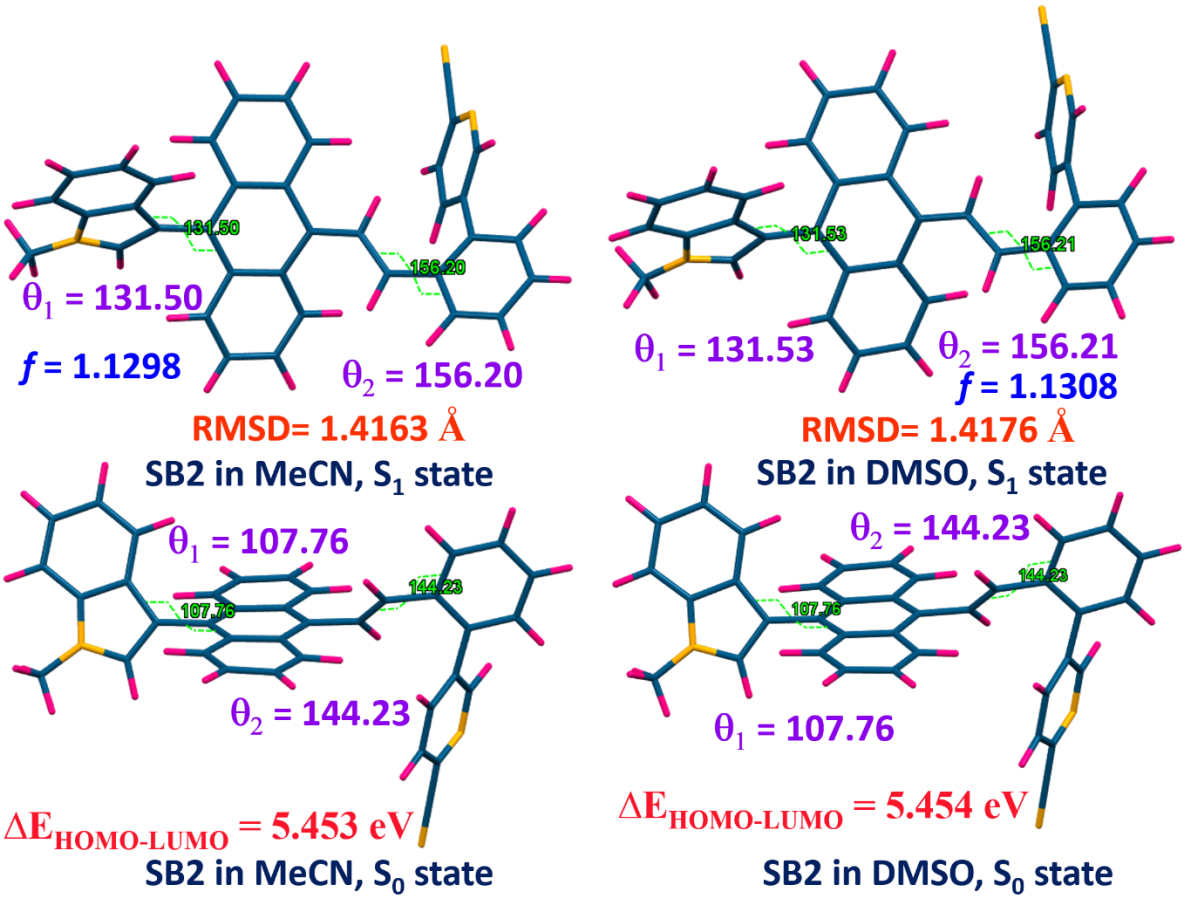

Fig. S3 TD-DFT optimized structures of **SB2** in MeCN and DMSO with selected torsion angles

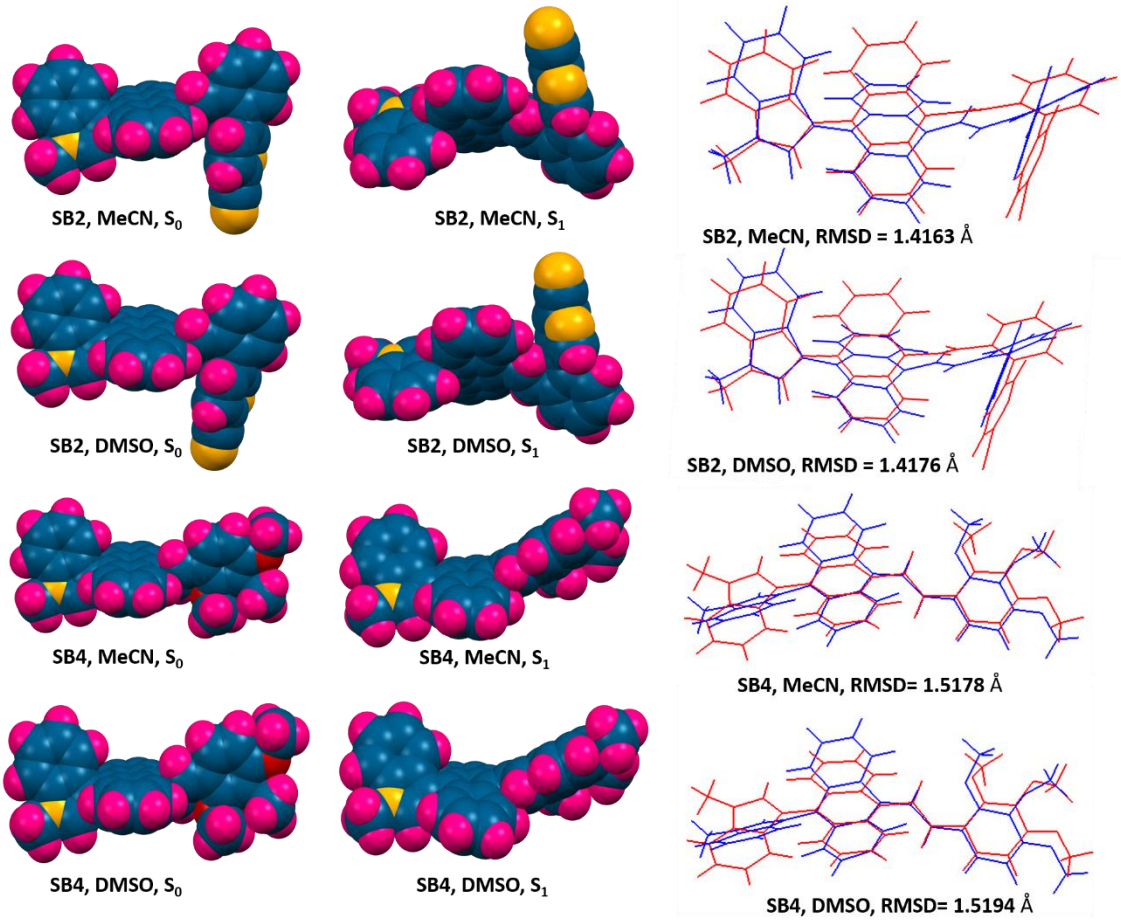

Fig. S4 Space fill presentations from the 'b' axis view of the TD-DFT optimized structures with the probable RMSD orientation

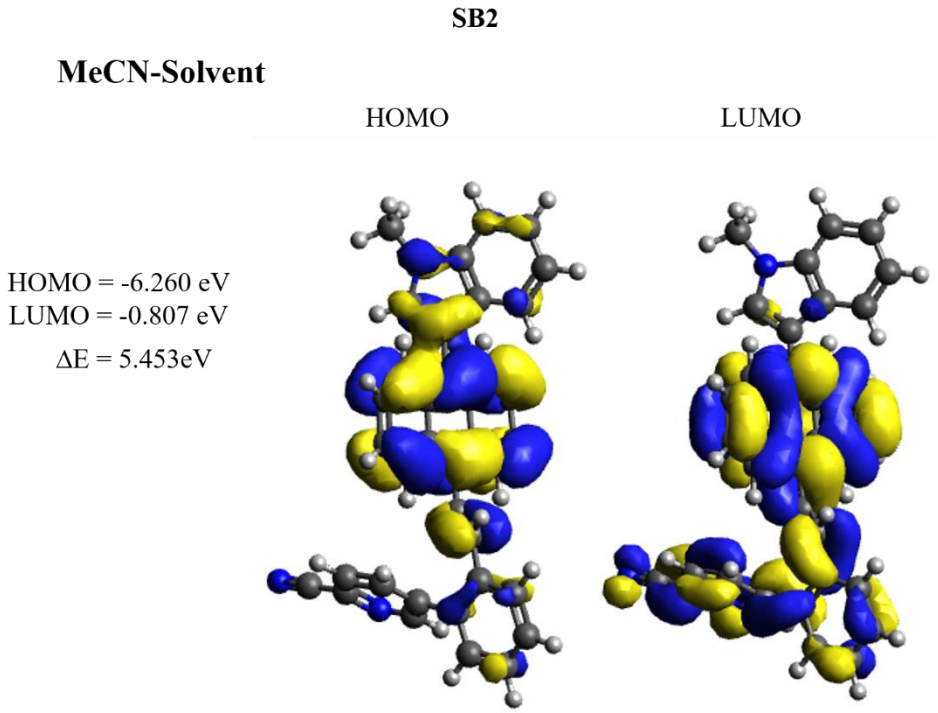

SB2

DMSO-Solvent

HOMO = -6.261eV
LUMO = -0.807 eV
ΔE = 5.454eV

HOMO

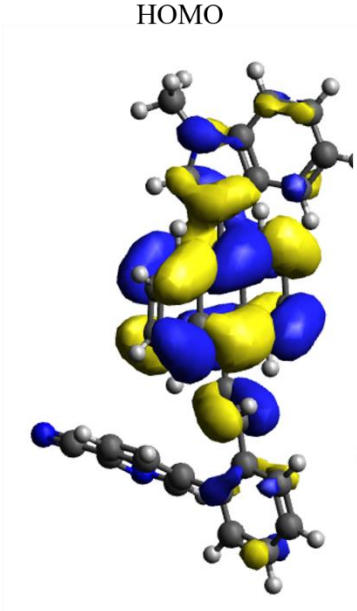

LUMO

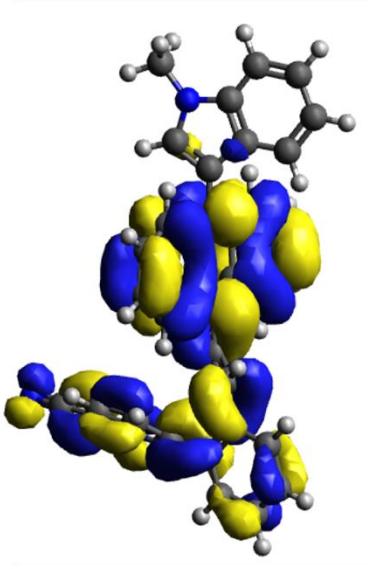

SB4

MeCN-Solvent

HOMO = -6.238 eV
LUMO = -0.612 eV
ΔE = 5.626 eV

HOMO

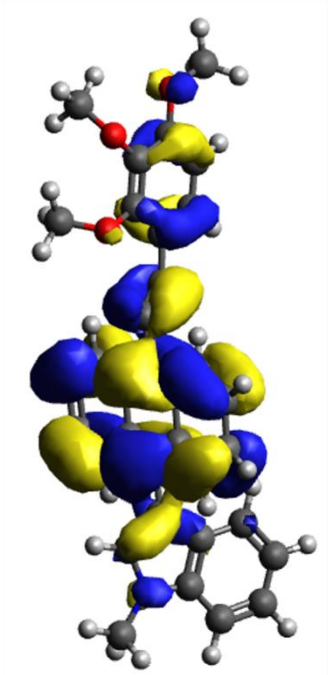

LUMO

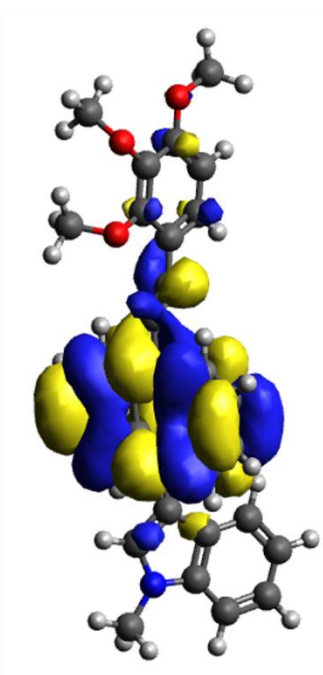

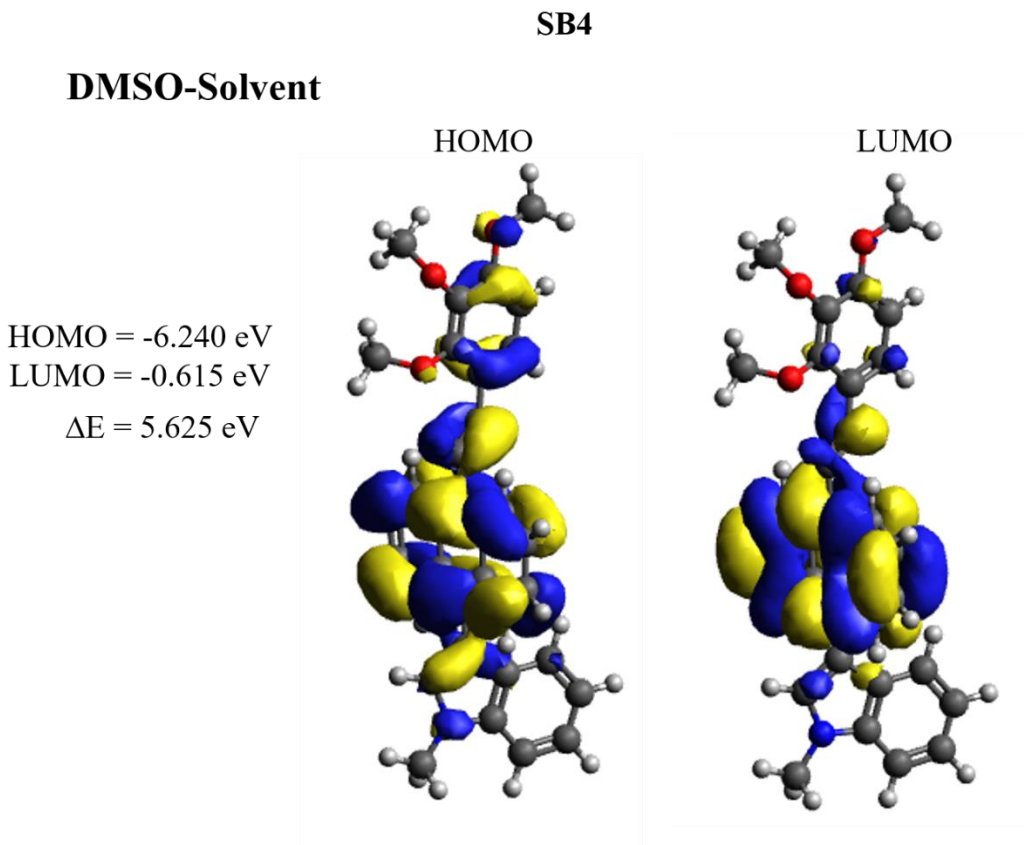

Fig. S5 HOMO-LUMO distribution of **SB2** and **SB4** in MeCN and DMSO

Table S3 TD-DFT calculation results for **SB2** and **SB4** in MecN and DMSO

Compound	Solvent	Absorbance Oscillator strength (*f'*)	Emission oscillator strength (*f*)	θ_1(°)	θ_2(°)	θ_1(°)	θ_2 (°)	RMSD (Å)	$\Delta E_{HOMO-LUMO}$ (eV)
SB2	MeCN	0.6546	1.1298	107.76	144.23	131.50	156.20	1.4163	5.453
SB2	DMSO	0.6726	1.1308	107.76	144.23	131.53	156.21	1.4176	5.454
SB4	MeCN	0.6522	1.2260	102.09	162.77	130.38	171.32	1.5178	5.626
SB4	DMSO	0.6691	1.2268	102.10	162.78	130.40	171.37	1.5194	5.625

Computational details: All density functional theoretical (DFT) calculations were performed using the ORCA Version 5.0.3 quantum chemical software package.[1,2] Ground state (S_0) geometry optimizations were done using DFT with CAM-B3LYP[3] functional and 6-31G* basis set. The excited stats (S_1) geometry optimization was done using time-dependent DFT (TDDFT). Root mean square deviation (RMSD) calculations were done using the Kabsch algorithm.[4] All structural and MOs were visualized using Avogadro software.[5]

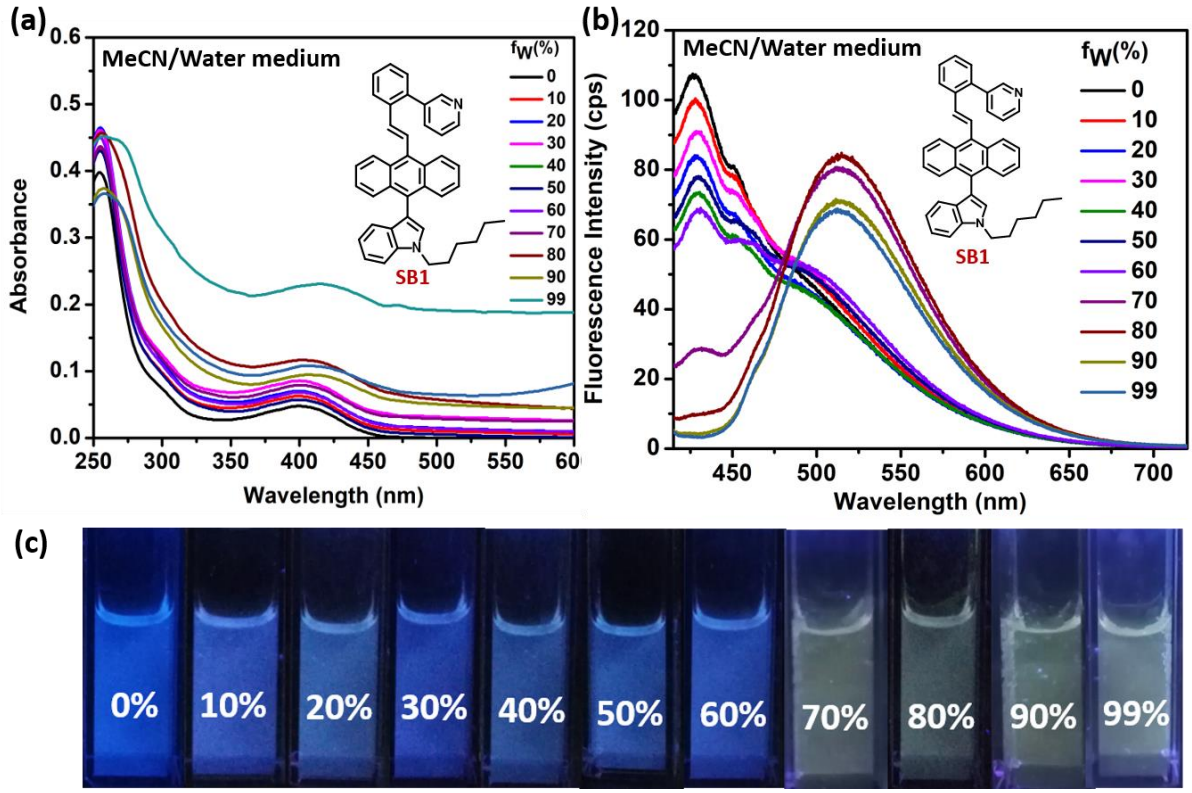

Fig. S6 non-AIE-property of **SB1** in MeCN/Water medium (a) absorbance (b) emission (c) visualization under 365nm UV-lamp

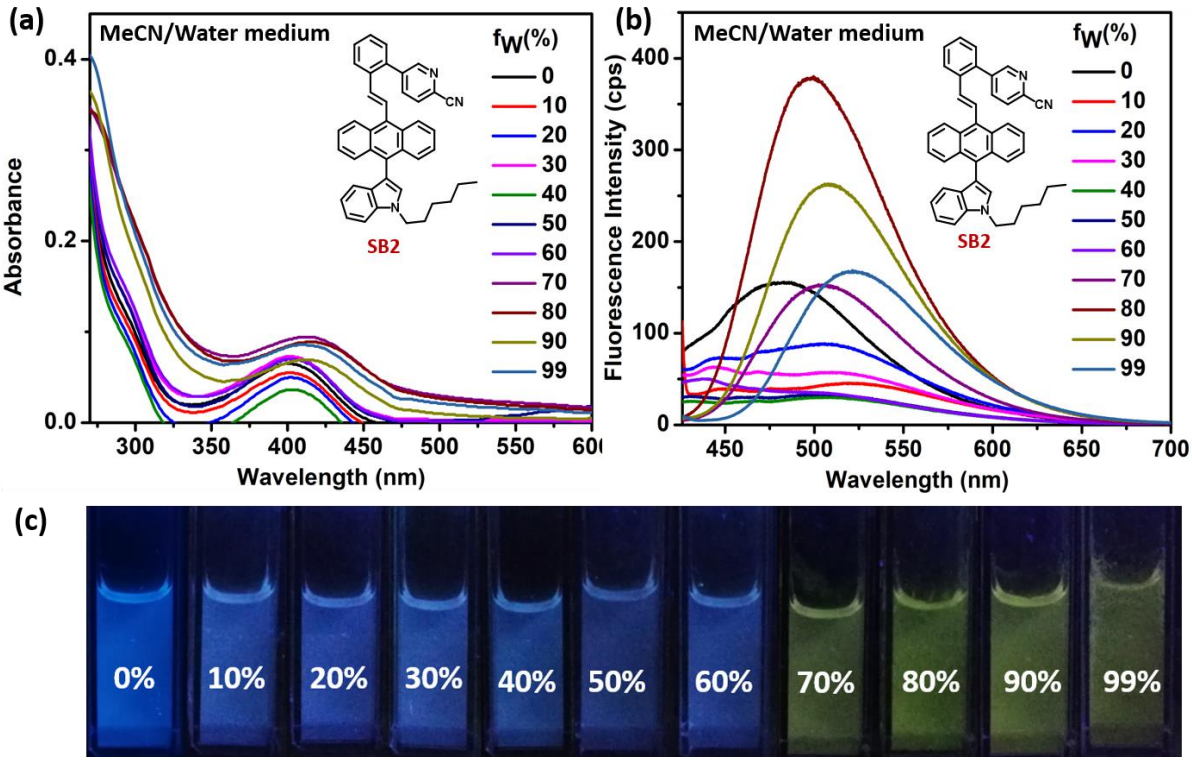

Fig. S7 Non-AIE-property of **SB2** in MeCN/Water medium (a) absorbance (b) emission (c) visualization under 365nm UV-lamp

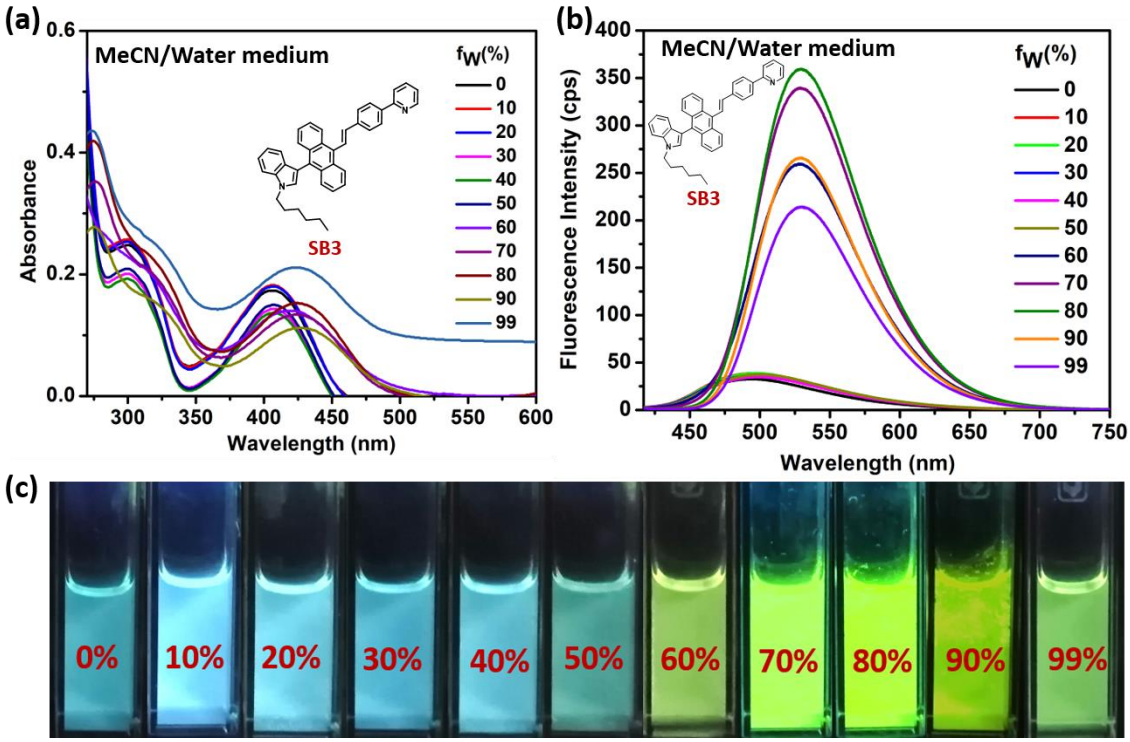

Fig. S8 AIE(E)-property of **SB3** in MeCN/Water medium (a) absorbance (b) emission (c) visualization under 365nm UV-lamp

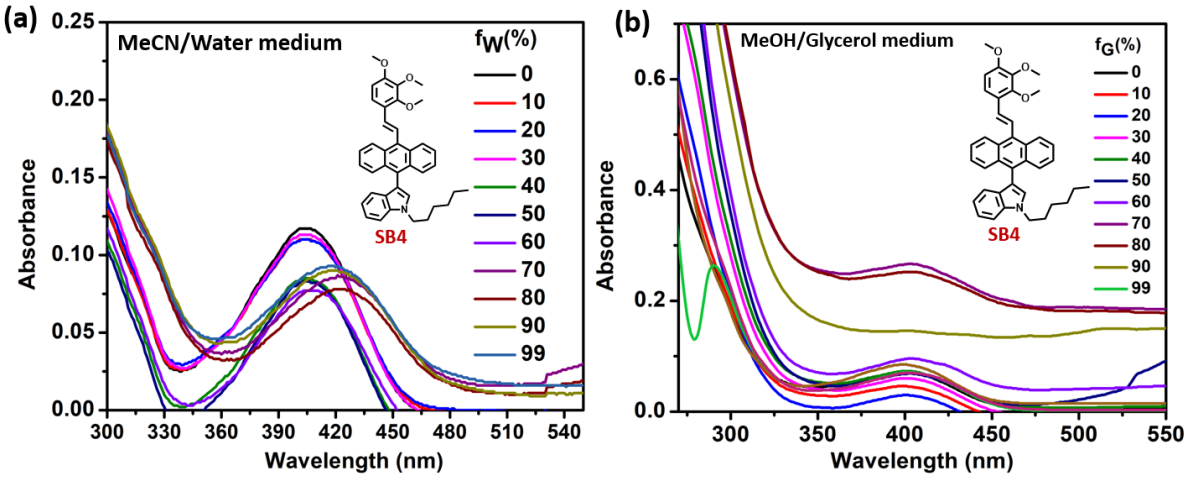

Fig. S9 (a) **SB4** absorbance in MeCN/water medium in different water fractions (b) **SB4** absorbance in MeOH/glycerol medium in different glycerol fraction

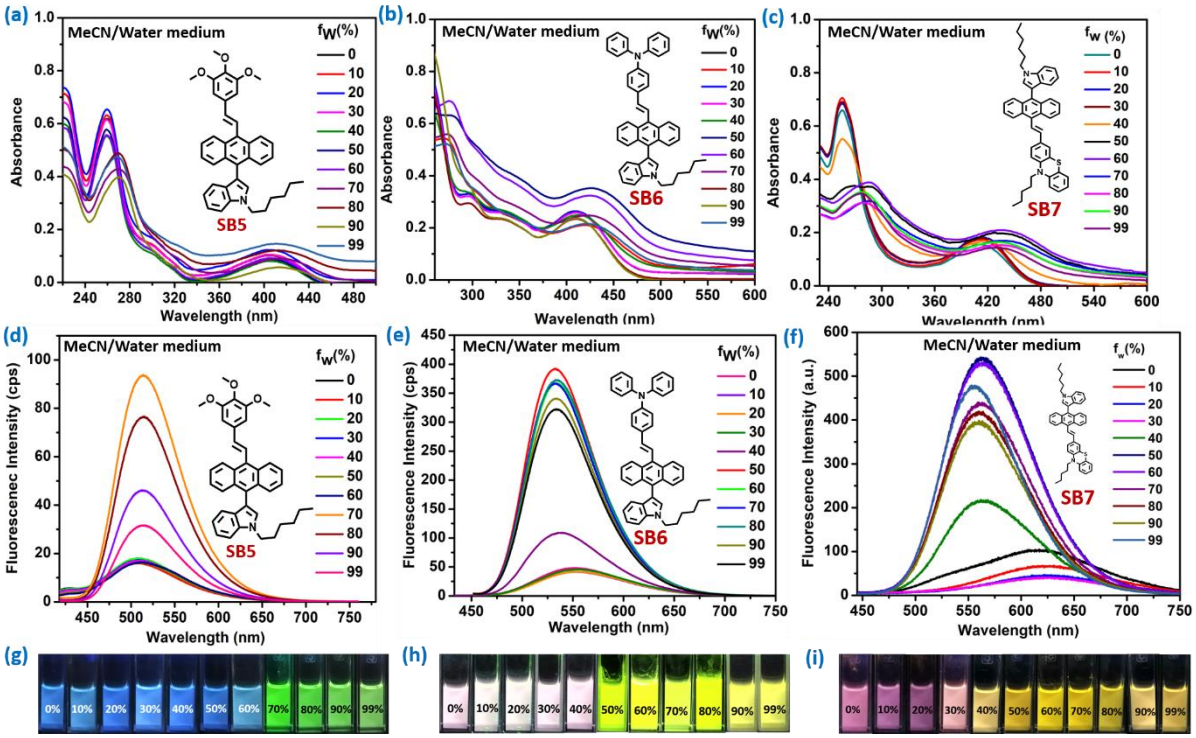

Fig. S10 AIE-properties of **SB5** (a,d,g), **SB6** (b,e,h) and **SB7**(c,f,i) in MeCN/water medium

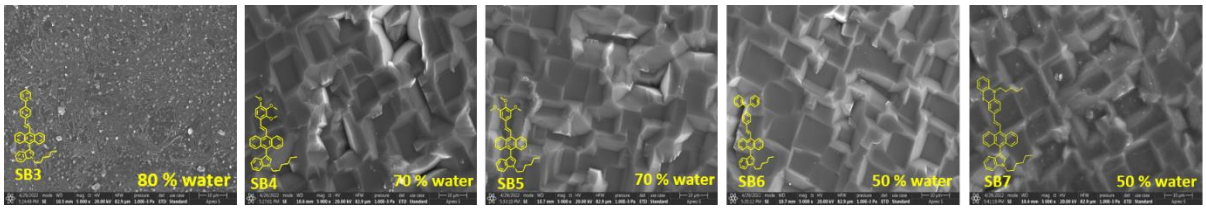

Fig. S11 SEM images of the AIE-gens at their respective water fraction for aggregation

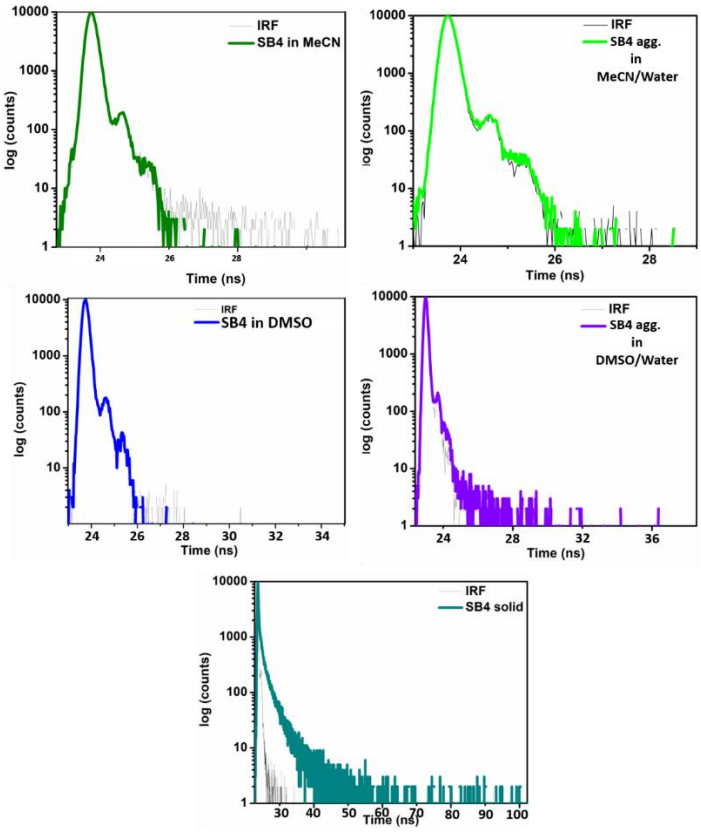

Fig. S12 Decay profile of SB4 in MeCN, DMSO, aggregates and solids

Table S4: Time-resolved fluorescence parameters for **SB4** as an SSOF-gen, DSE-gen, and AIEE-gen

Form	χ 2	τ_1	τ_2	τ_3	α1	α2	α3	$\tau_{avg.}$ (ns))	k_r (x 10^9 s^{-1})	k_{nr} (x 10^9 s^{-1})	k_r/k_{nr}
In MeCN	1.0351	0.0277	0.3848	-	0.9995	0.0005	-	0.0279	0.907	34.9	0.026
Aggregate in MeCN/Water medium	0.9909	0.0614	0.4265		0.9866	0.0134	-	0.0663	61.4	14.5	4.234
In DMSO	1.0282	0.0907	0.0432	0.6831	0.0555	0.9436	0.0009	0.0464	0.47	21.1	0.022
Aggregate in DMSO/Water medium	1.0206	0.0787	0.0466	-	0.1052	0.8948	-	0.0500	66.2	19.3	3.43
Solid-state	0.9915	0.7666	3.004	0.0509	0.0176	0.0004	0.9779	0.0766	1.34	11.7	0.11

The average lifetime was obtained by fitting the decay profiles to a tri/bi-exponential function eqn-1.

Fit = $A_1.exp\ (-t/\ \tau_1) + A_2.exp\ (-t/\ \tau_2) + A_3.exp\ (-t/\ \tau_3)$ …….. (eq-1)

α_1, α_2 are weighted components and τ_1, τ_2, τ_3 are individual lifetime components of the decay. The qualities of the fit were determined by judging the chi square (χ^2) values.

The rate constants are calculated using: $k_r = [\Phi_f / \boldsymbol{\tau_{avg}}]\ s^{-1}$; $k_{nr} = [1-\Phi_f / \boldsymbol{\tau_{avg}}]\ s^{-1}$

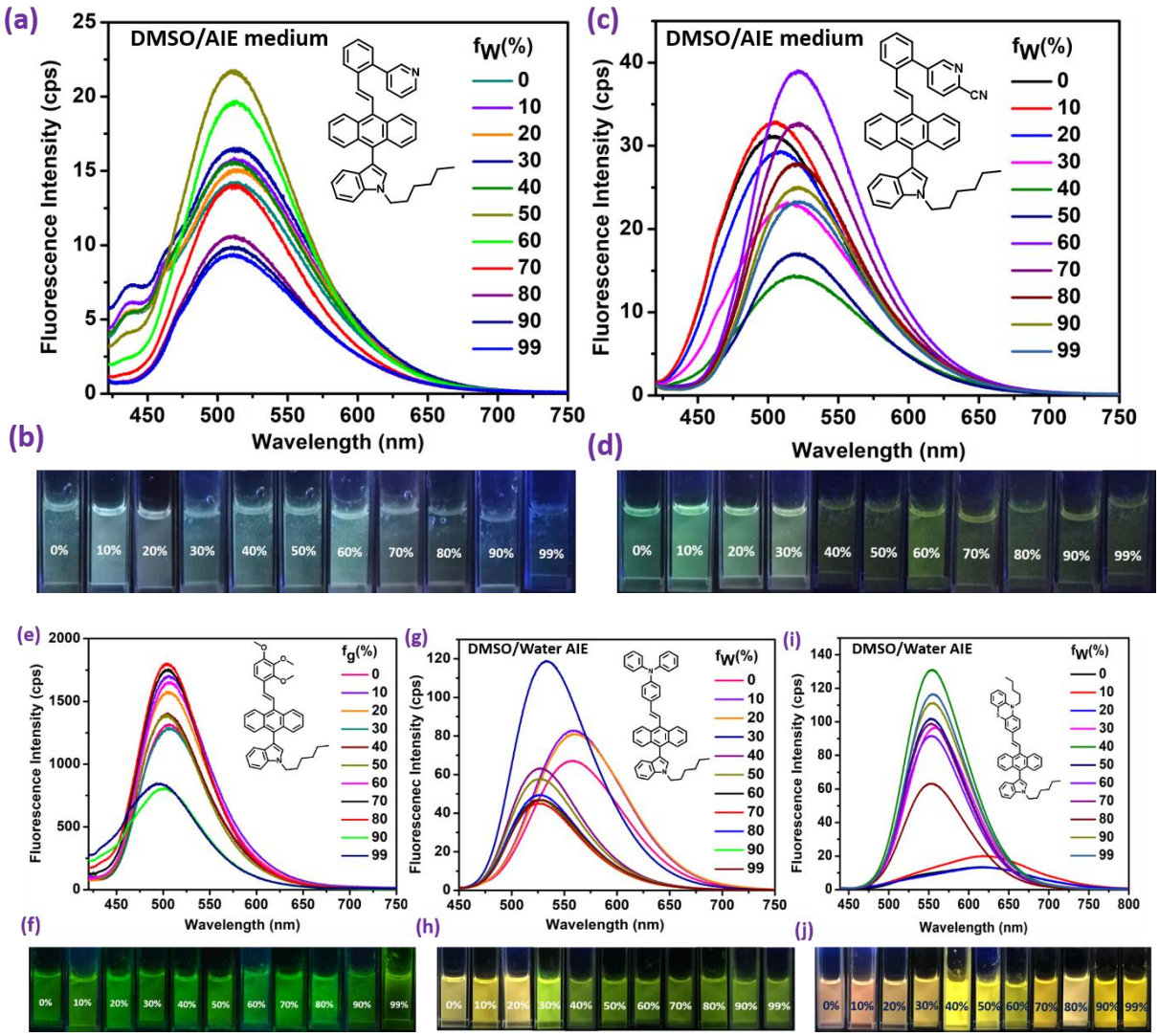

Fig. S13 Aggregation-induced enhanced emission property of **SB1** (a-b)**, SB2** (c-d)**, SB4** (e-f)**, SB6** (g-h), and **SB7** (i-j) in DMSO/Water medium. The pictures had been taken by keeping the containers under a 365nm UV lamp. The excitation wavelengths were between 408 nm to 424 nm for them.

FaDu 4h DAPI vs SB4

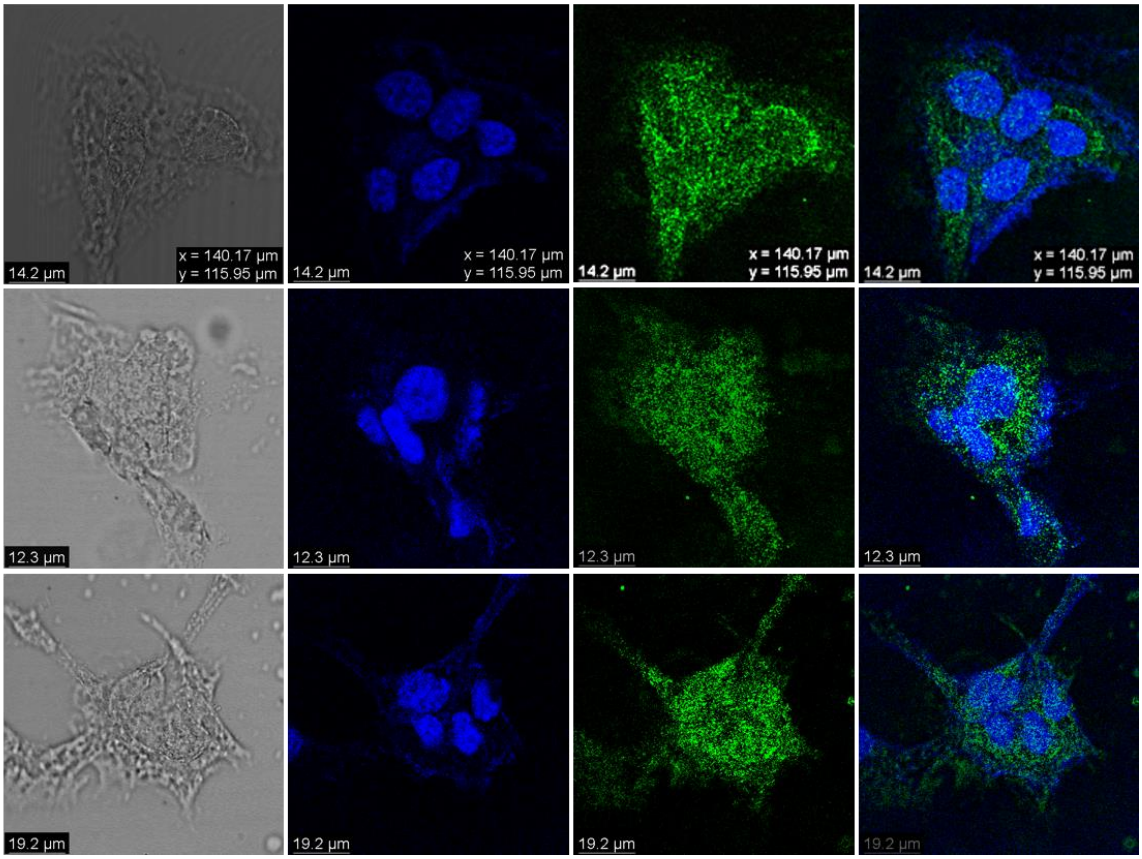

FaDu 4h DAPI vs DOX

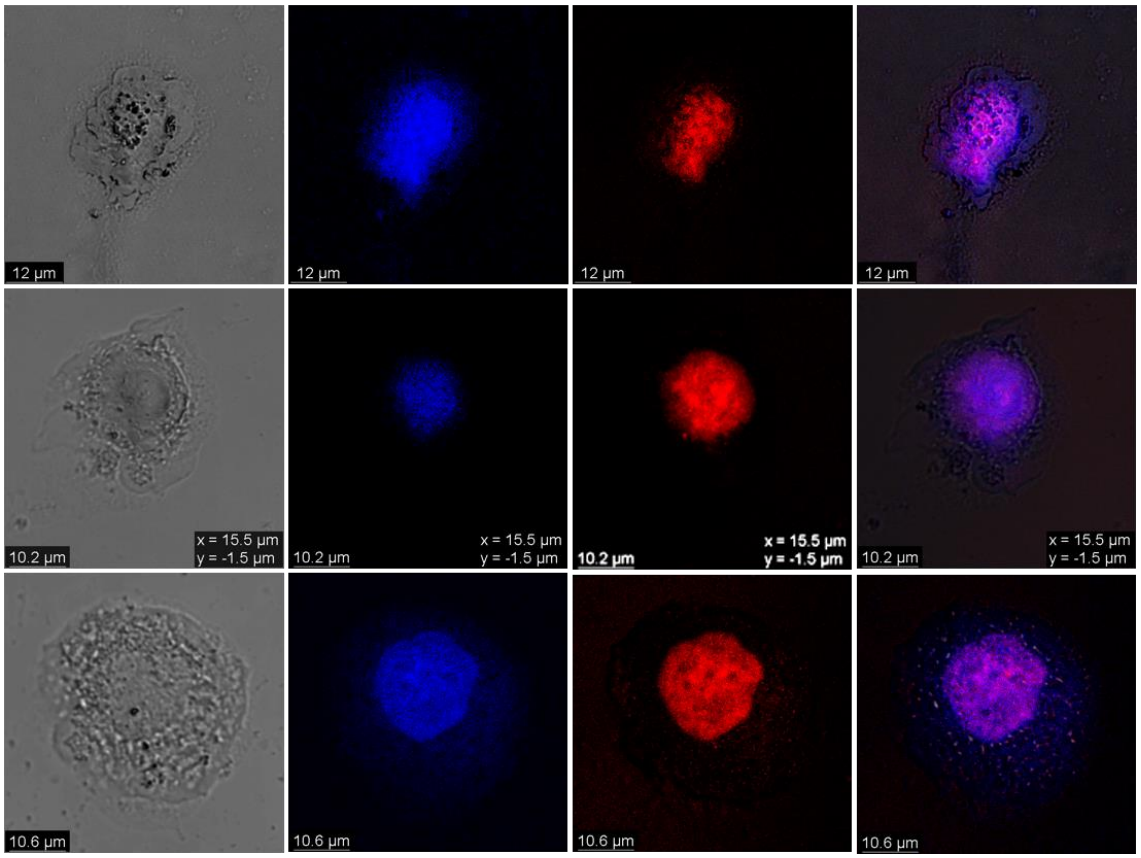

FaDu 24h DAPI vs SB4

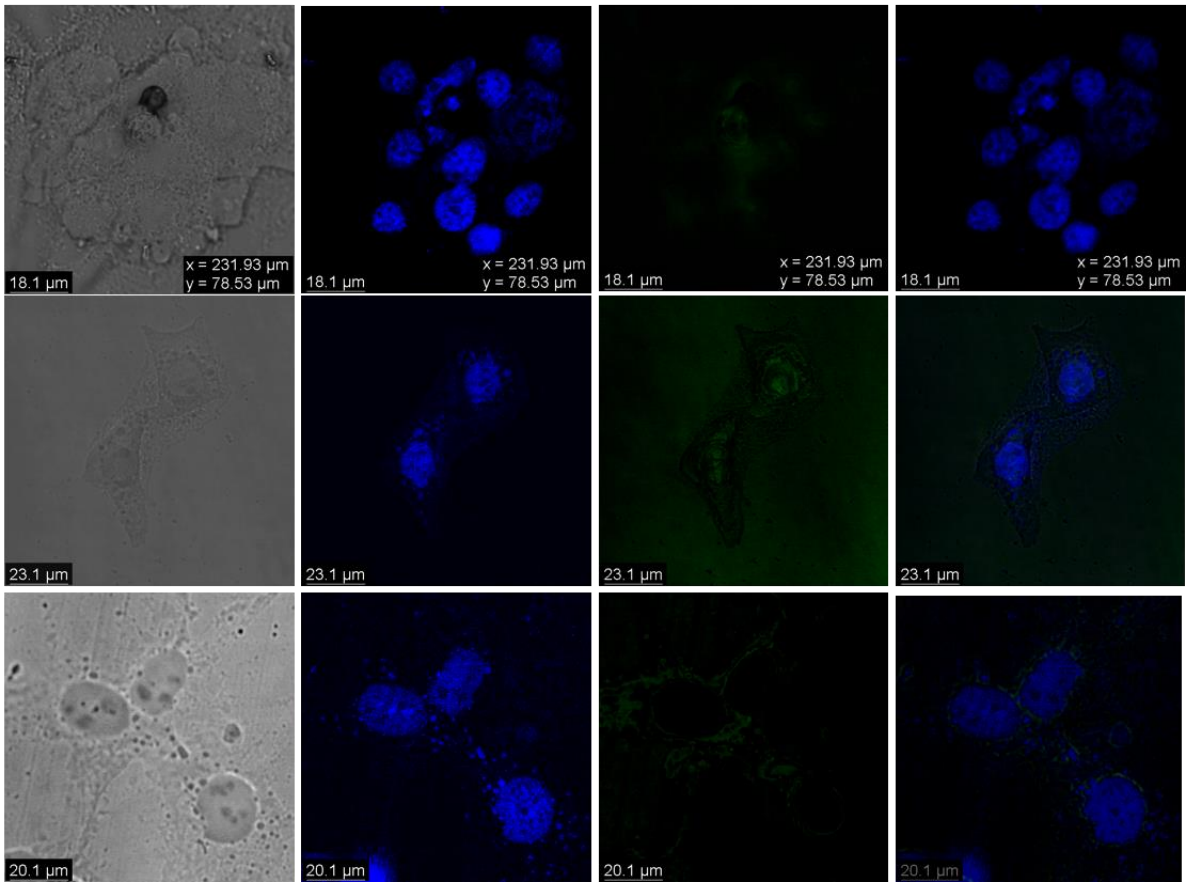

FaDu 24h DAPI vs DOX

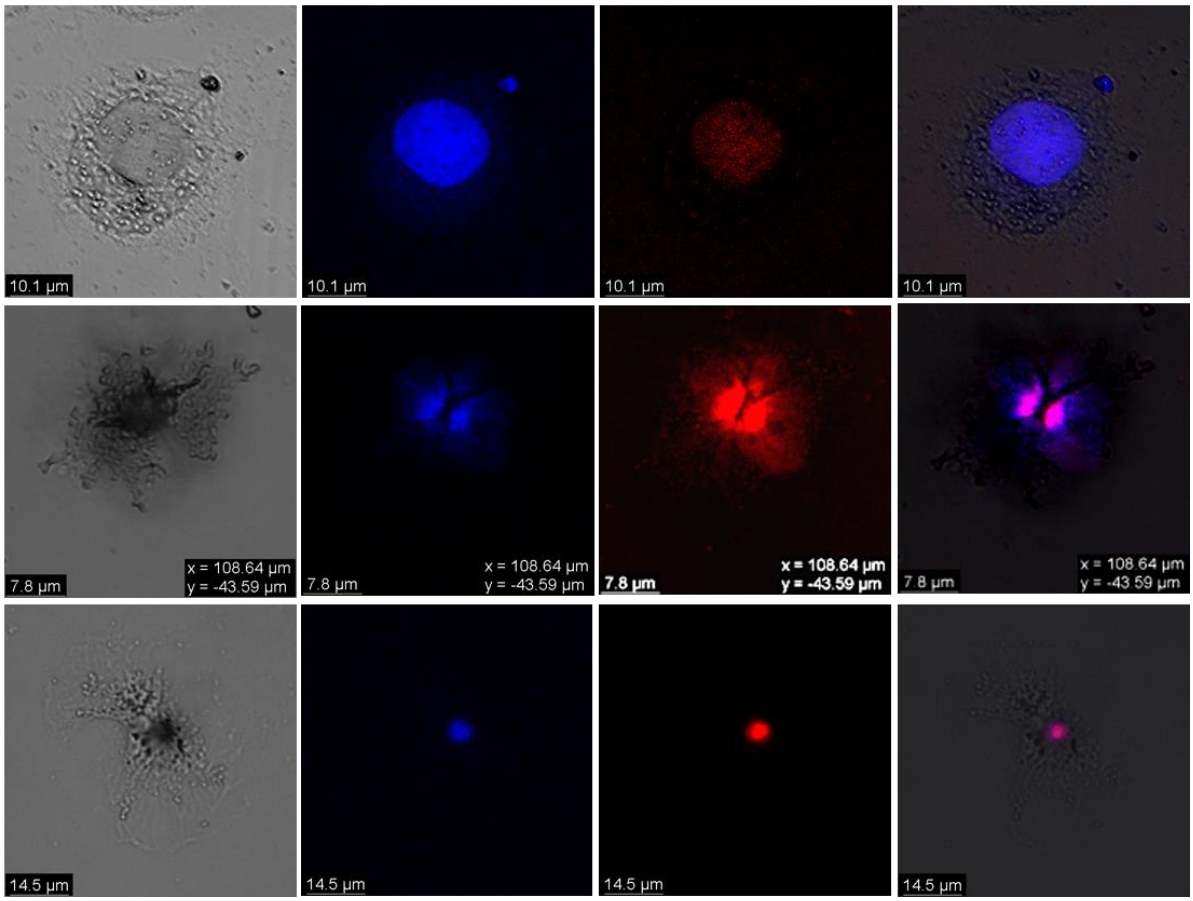

4T1 4h DAPI vs SB4

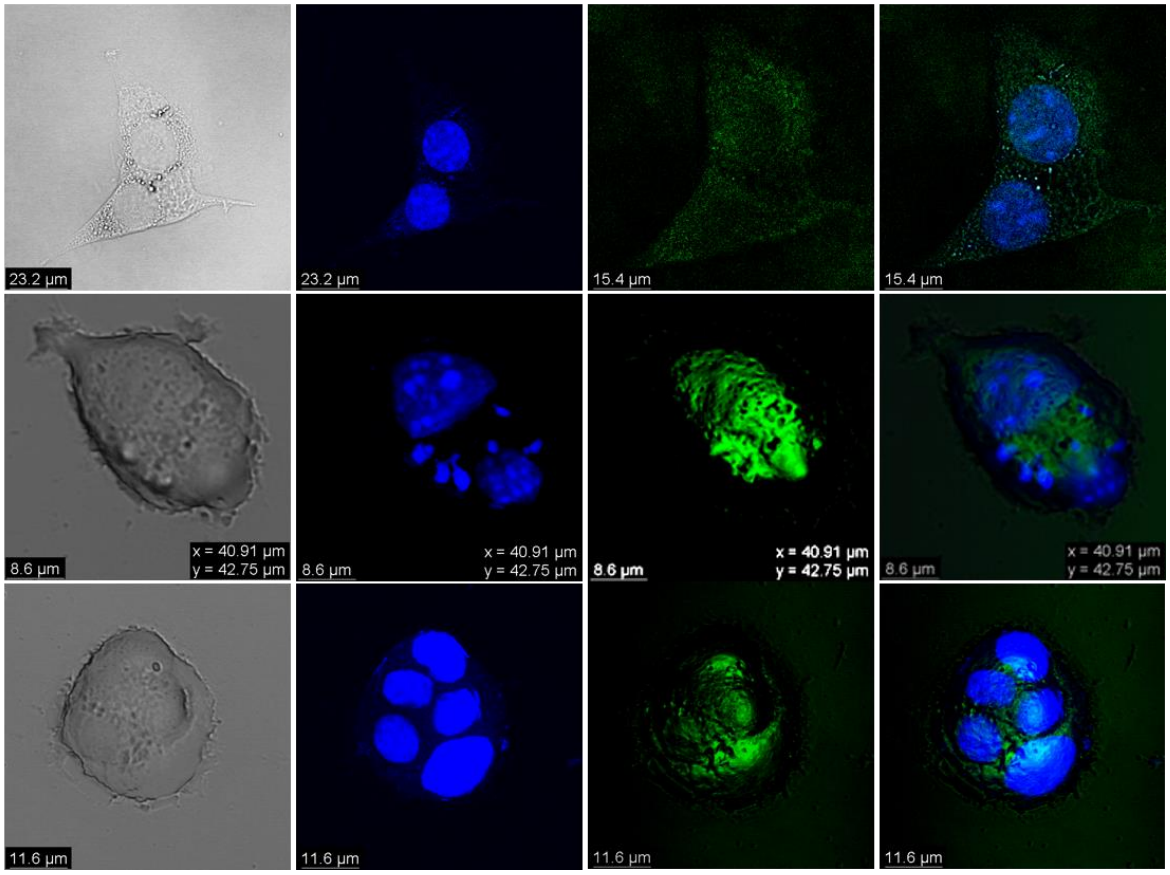

4T1 4h DAPI vs DOX

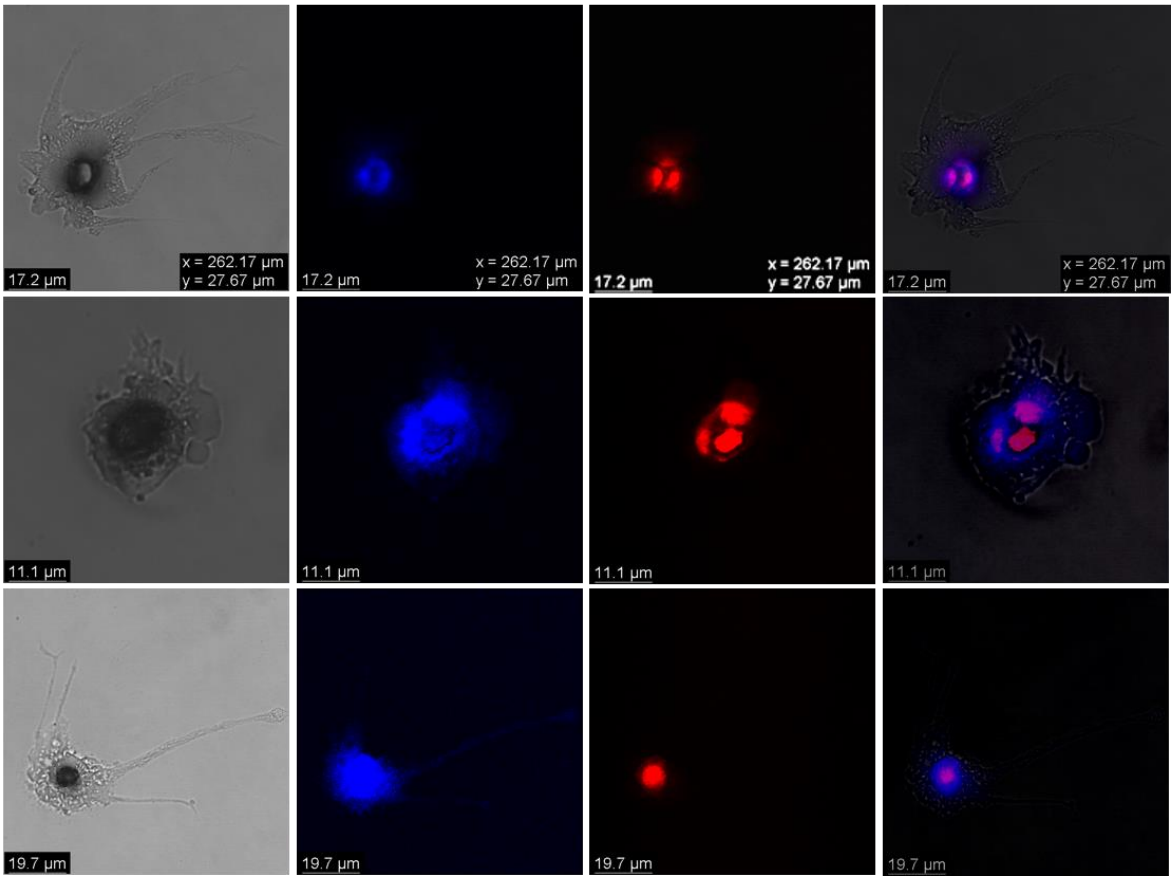

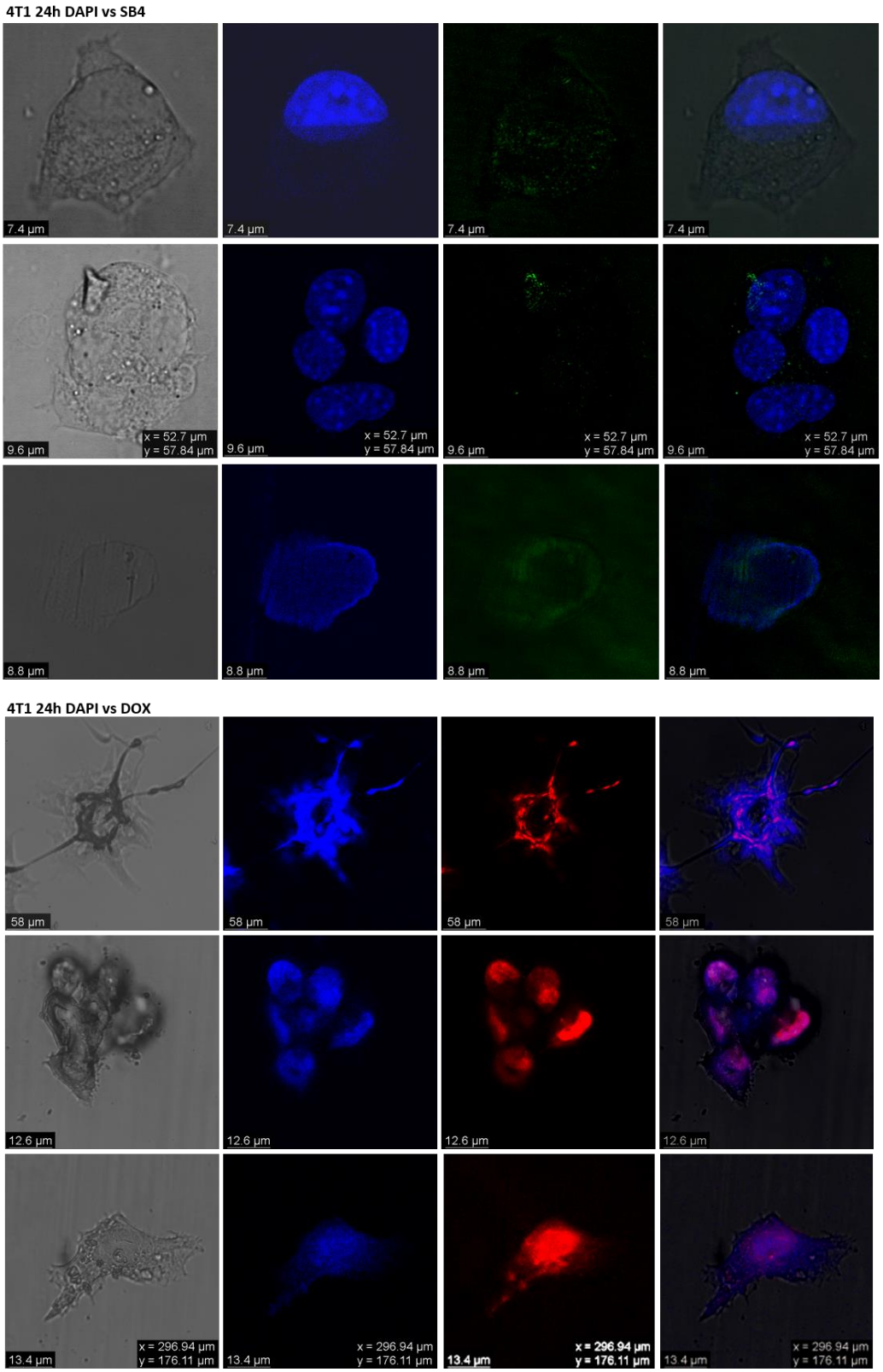

Fig. S14 Confocal images utilized for quantification. The blue color is displayed by DAPI, red by doxorubicin, and green by SB4, and the mixed color appears by colocalization

(a) 3PP0 with reported ligand

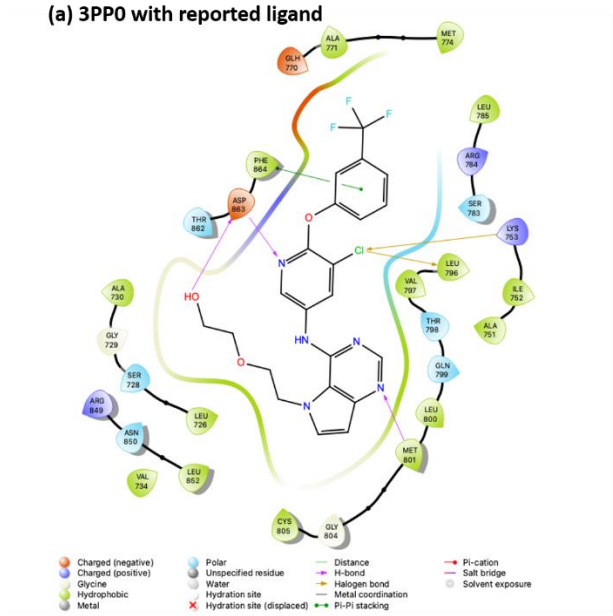

(b) 3PP0 with SB4

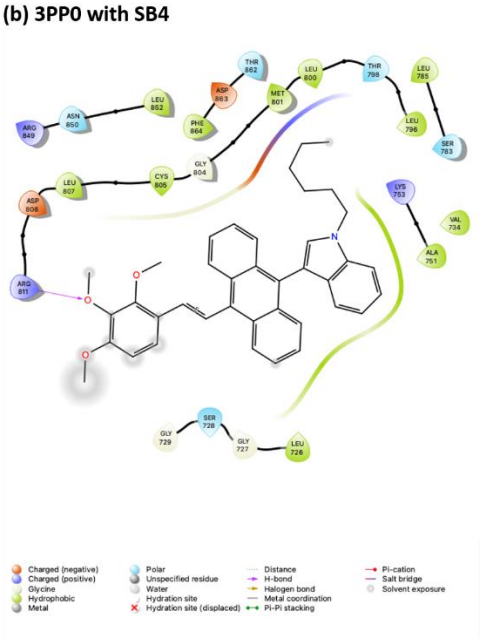

(c) 7JXH with reported ligand

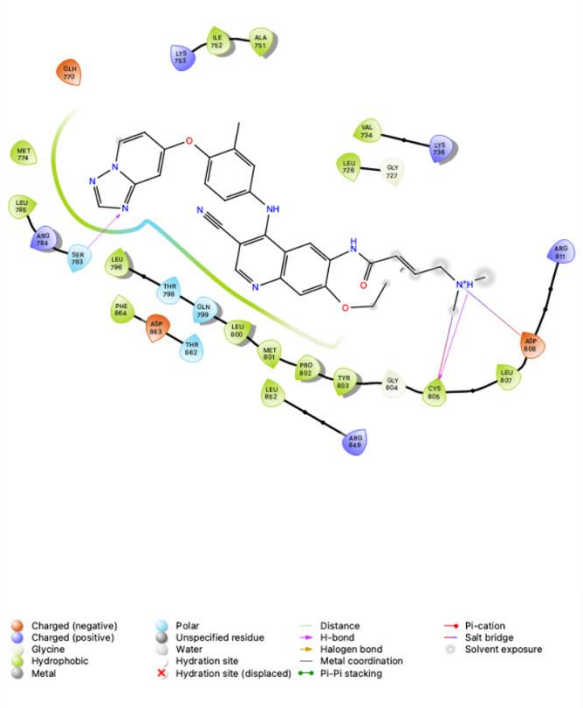

(d) 7JXH with SB4

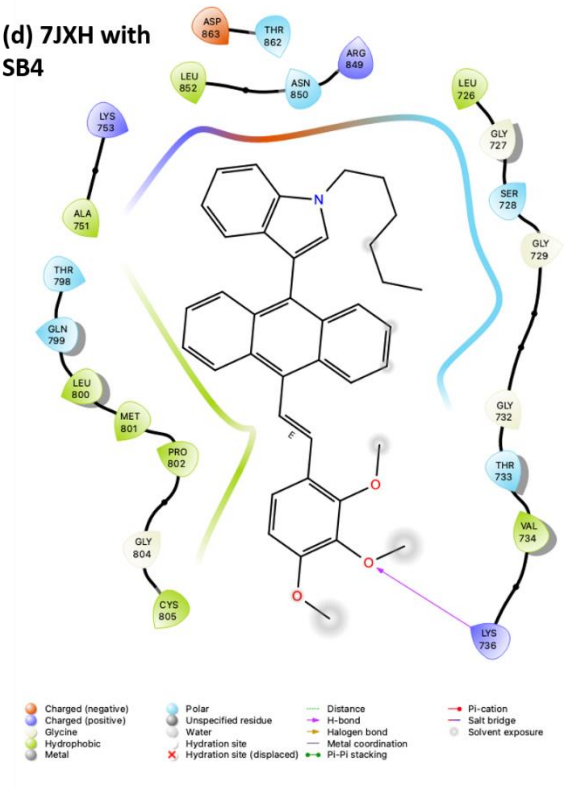

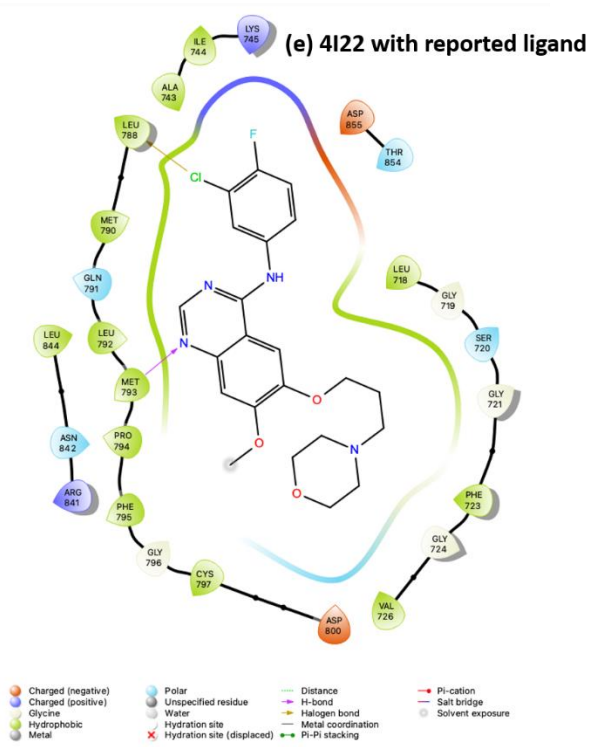
(e) 4I22 with reported ligand
LYS 745
ILE 744
ALA 743
LEU 788
ASP 855
THR 854
MET 790
GLN 791
LEU 844
LEU 792
MET 793
ASN 842
PRO 794
ARG 841
PHE 795
GLY 796
CYS 797
ASP 800
VAL 726
GLY 724
PHE 723
GLY 721
SER 720
GLY 719
LEU 718
Charged (negative)
Charged (positive)
Glycine
Hydrophobic
Metal
Polar
Unspecified residue
Water
Hydration site
Hydration site (displaced)
Distance
H-bond
Halogen bond
Metal coordination
Pi-Pi stacking
Pi-cation
Salt bridge
Solvent exposure

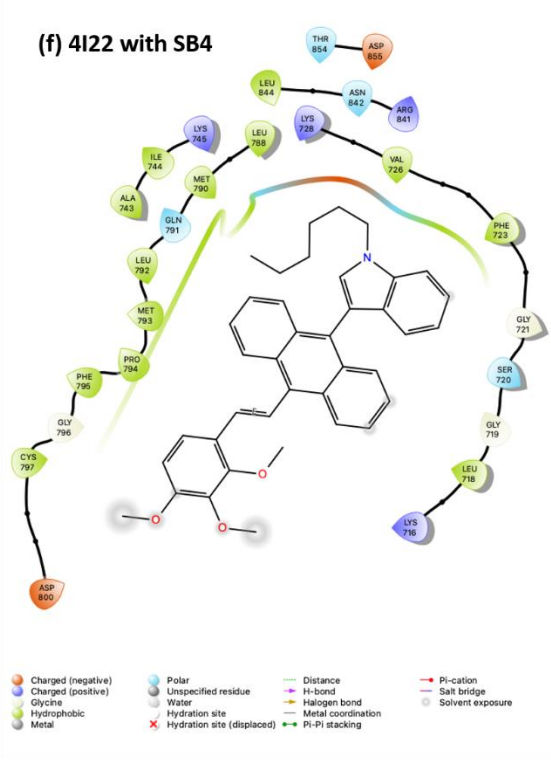
(f) 4I22 with SB4
THR 854
ASP 855
LEU 844
ASN 842
ARG 841
LYS 728
LEU 788
LYS 745
ILE 744
MET 790
ALA 743
GLN 791
VAL 726
PHE 723
LEU 792
MET 793
PRO 794
PHE 795
GLY 796
CYS 797
ASP 800
GLY 721
SER 720
GLY 719
LEU 718
LYS 716
Charged (negative)
Charged (positive)
Glycine
Hydrophobic
Metal
Polar
Unspecified residue
Water
Hydration site
Hydration site (displaced)
Distance
H-bond
Halogen bond
Metal coordination
Pi-Pi stacking
Pi-cation
Salt bridge
Solvent exposure

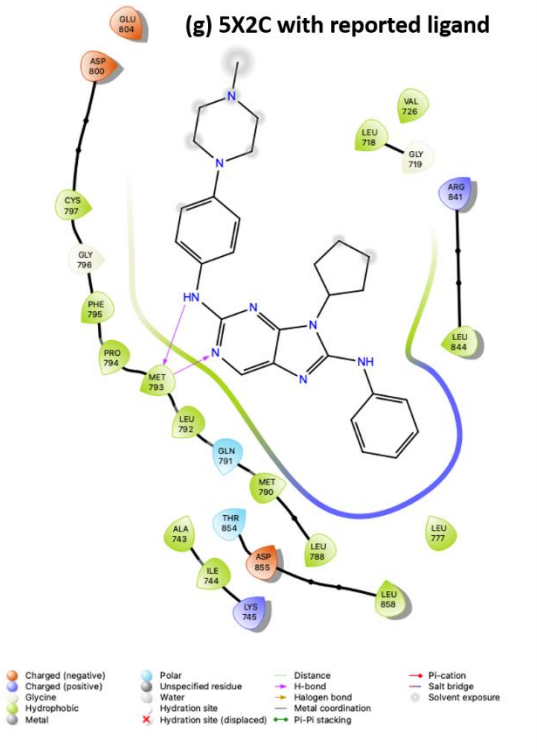
(g) 5X2C with reported ligand
GLU 804
ASP 800
CYS 797
GLY 796
PHE 795
PRO 794
MET 793
LEU 792
GLN 791
MET 790
ALA 743
THR 854
ILE 744
ASP 855
LYS 745
LEU 788
LEU 858
LEU 777
LEU 844
ARG 841
LEU 718
GLY 719
VAL 726
Charged (negative)
Charged (positive)
Glycine
Hydrophobic
Metal
Polar
Unspecified residue
Water
Hydration site
Hydration site (displaced)
Distance
H-bond
Halogen bond
Metal coordination
Pi-Pi stacking
Pi-cation
Salt bridge
Solvent exposure

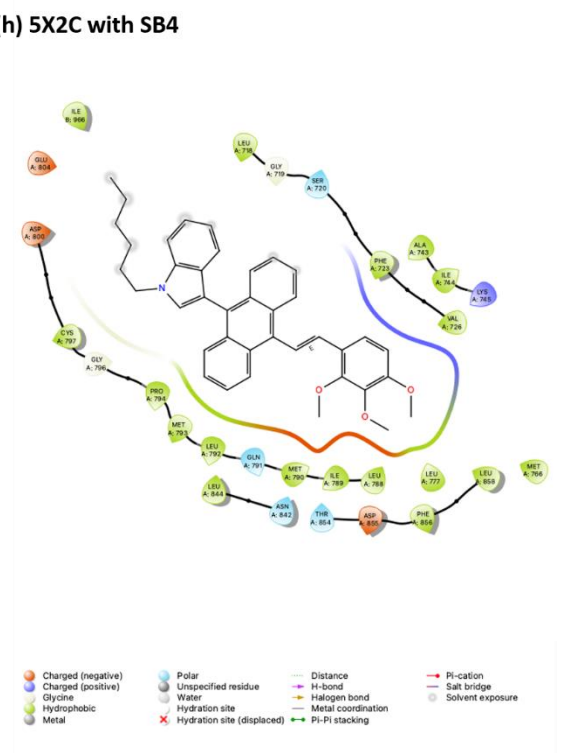
(h) 5X2C with SB4
Charged (negative)
Charged (positive)
Glycine
Hydrophobic
Metal
Polar
Unspecified residue
Water
Hydration site
Hydration site (displaced)
Distance
H-bond
Halogen bond
Metal coordination
Pi-Pi stacking
Pi-cation
Salt bridge
Solvent exposure

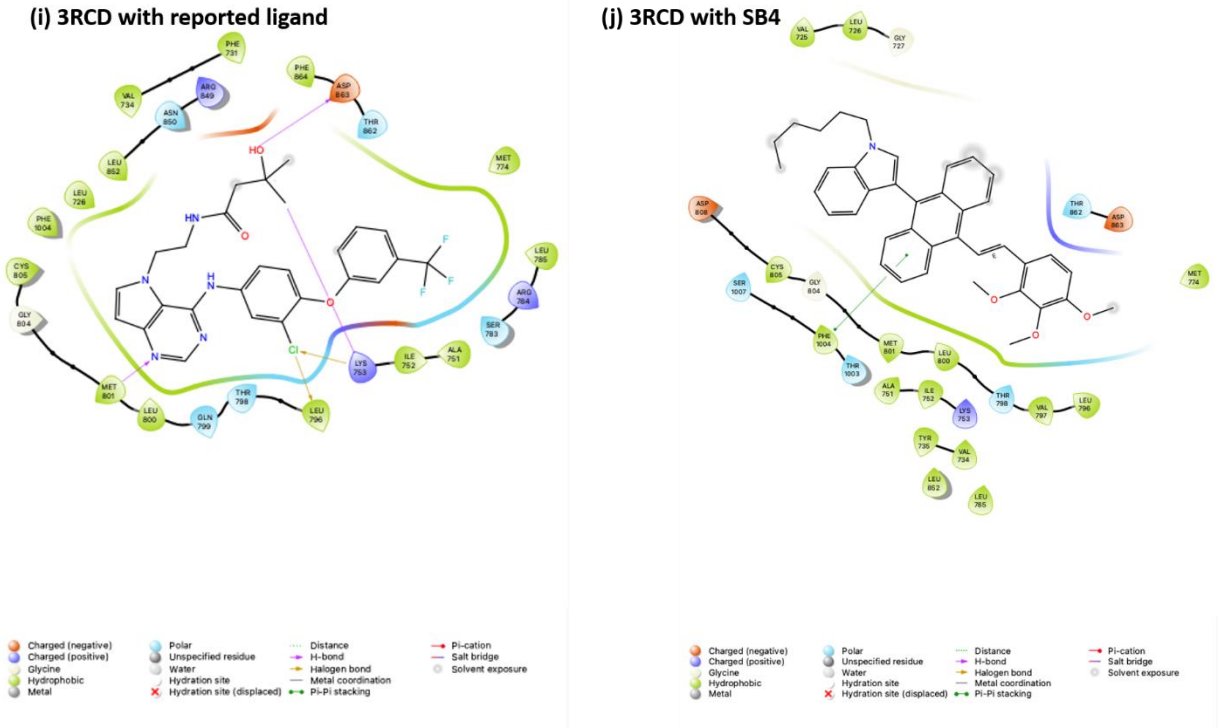

Fig. S15 2D view of interactions of reported ligands and **SB4**

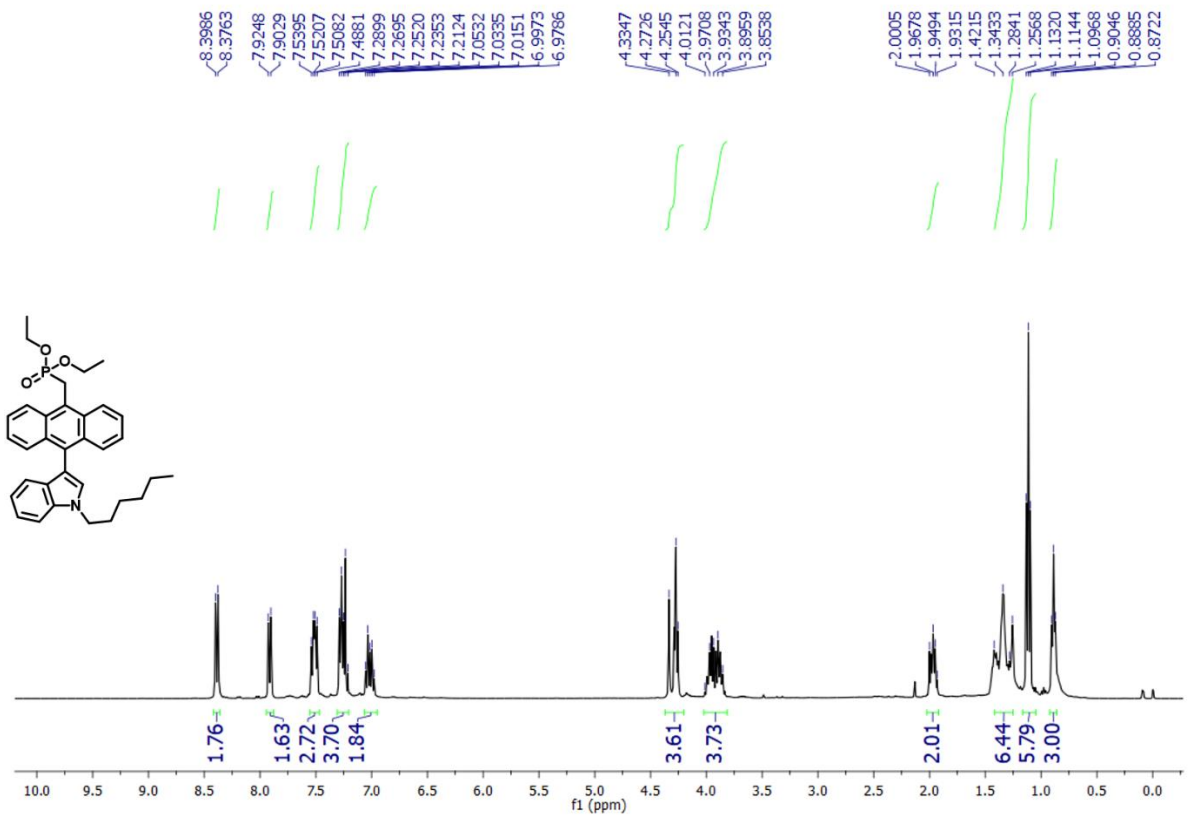

Fig. S16 ^{1}H NMR spectra of diethyl ((10-(1-hexyl-1H-indol-3-yl)anthracen-9-yl)methyl)phosphonate

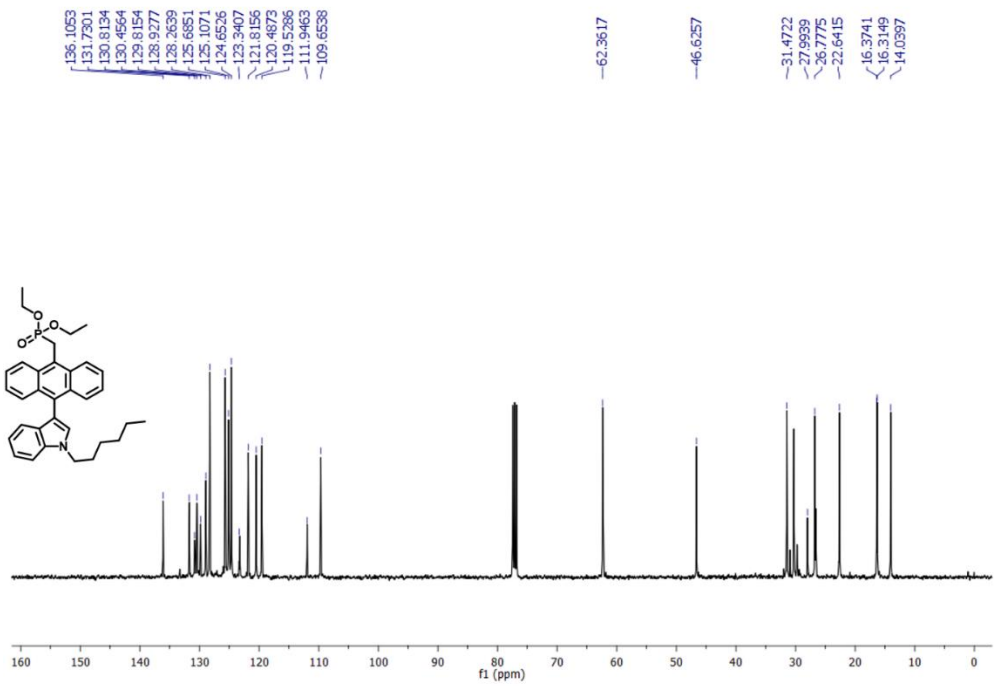

Fig. S17 ^{13}C NMR spectra of diethyl ((10-(1-hexyl-1H-indol-3-yl)anthracen-9-yl)methyl)phosphonate

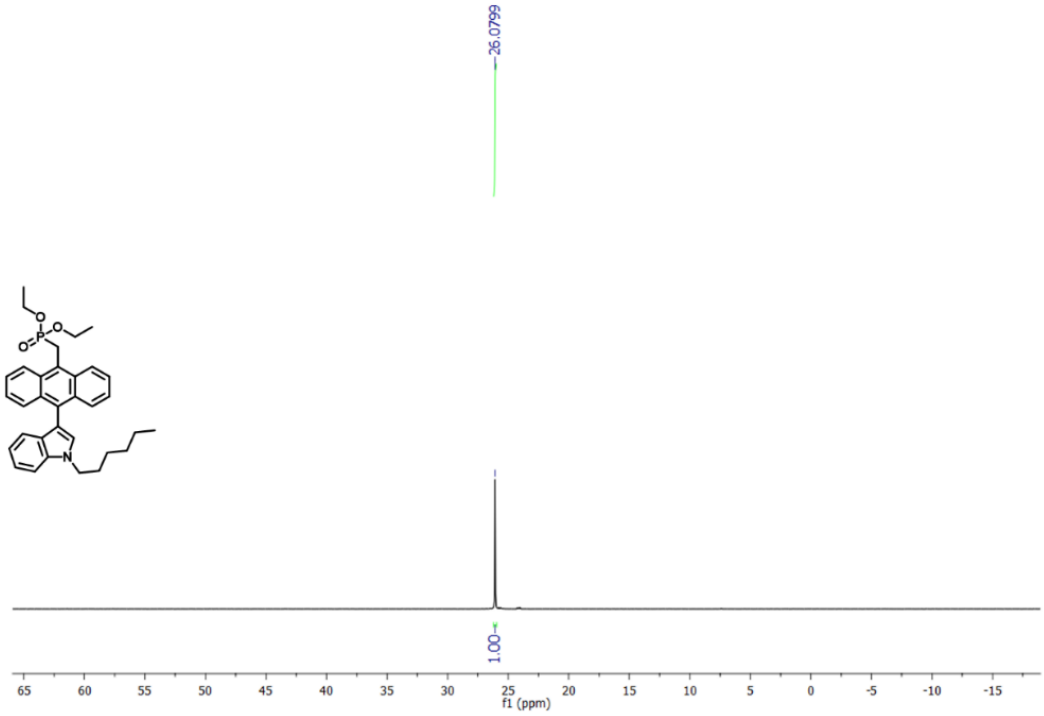

Fig. S18 ^{31}P NMR spectra of diethyl ((10-(1-hexyl-1H-indol-3-yl)anthracen-9-yl)methyl)phosphonate

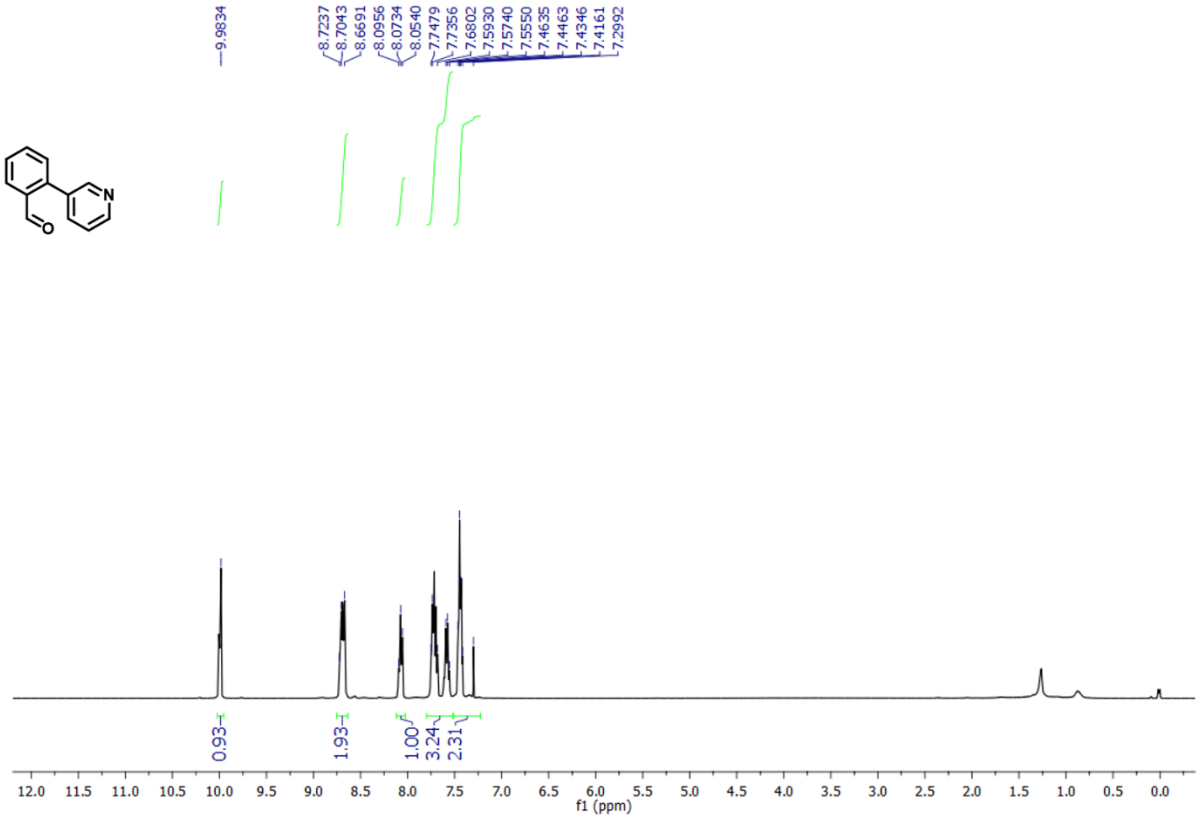

Fig. S19 ^{1}H NMR spectra of 2-(pyridin-3-yl)benzaldehyde

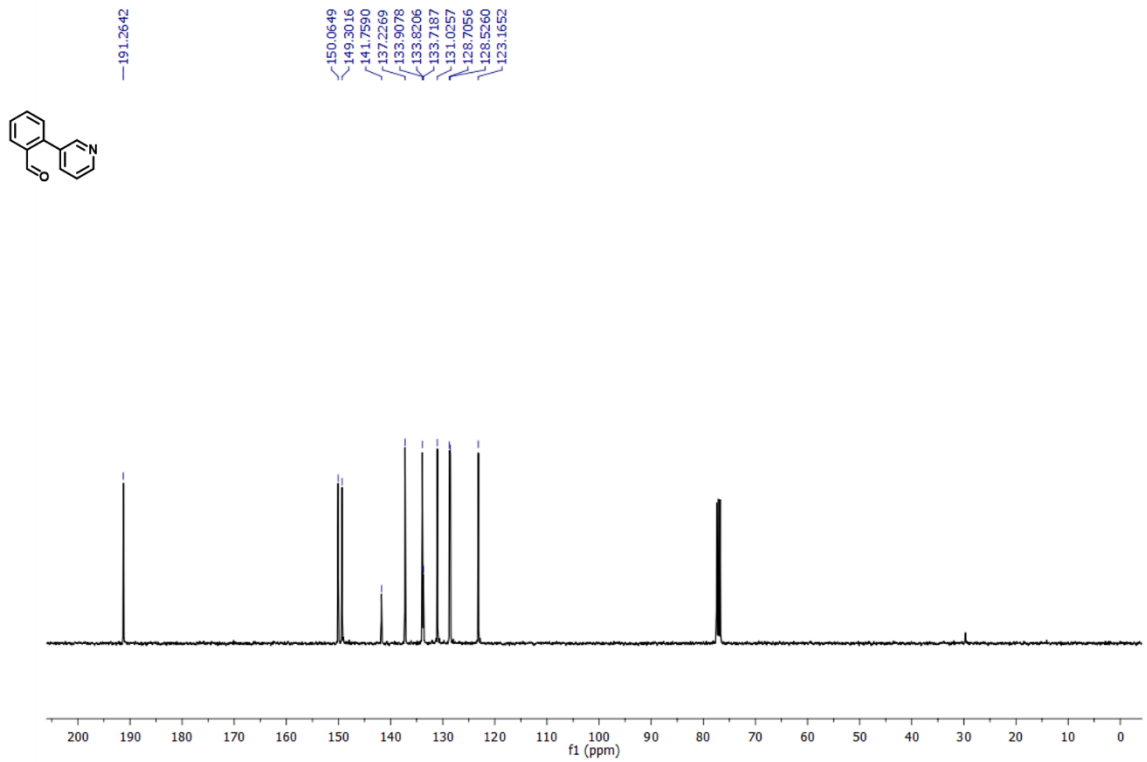

Fig. S20 ^{13}C NMR spectra of 2-(pyridin-3-yl)benzaldehyde

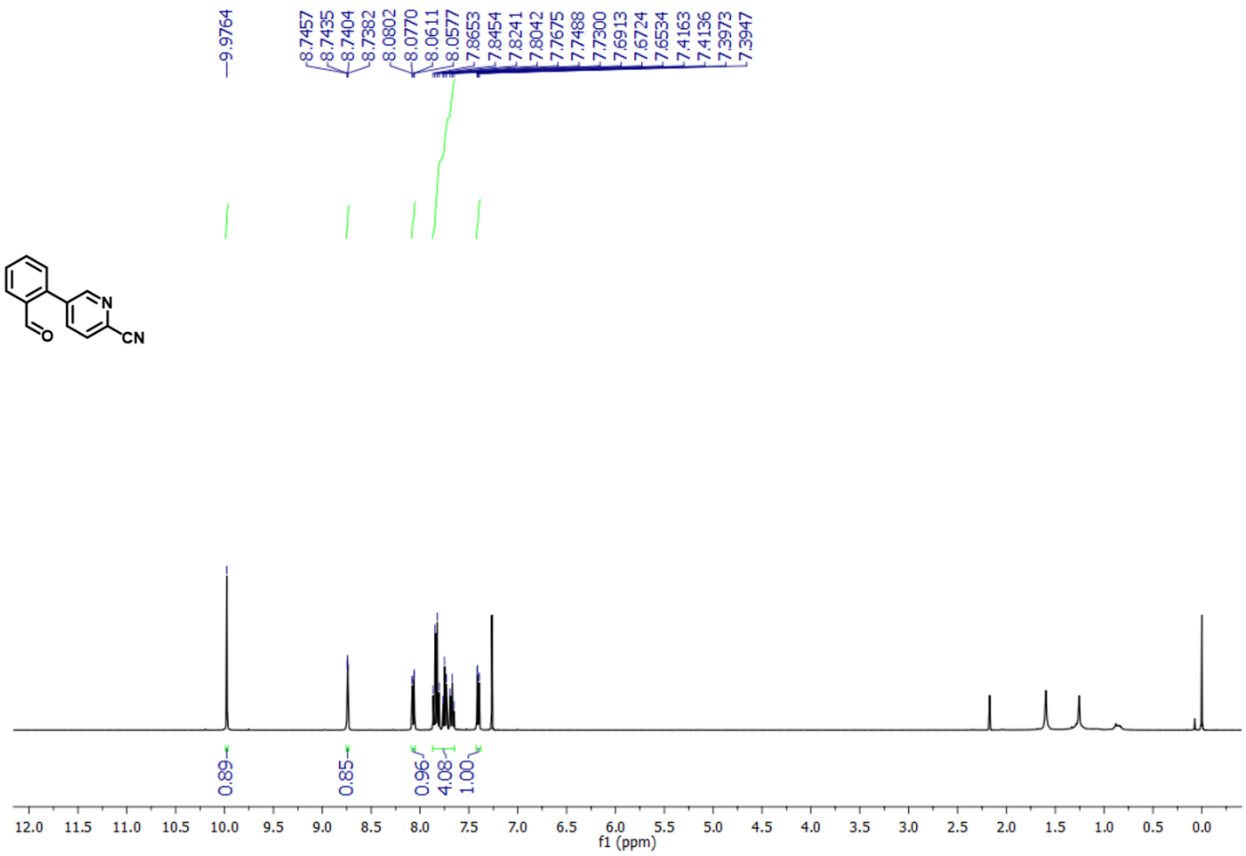

Fig. S21 ^{1}H NMR spectra of 5-(2-formylphenyl)picolinonitrile

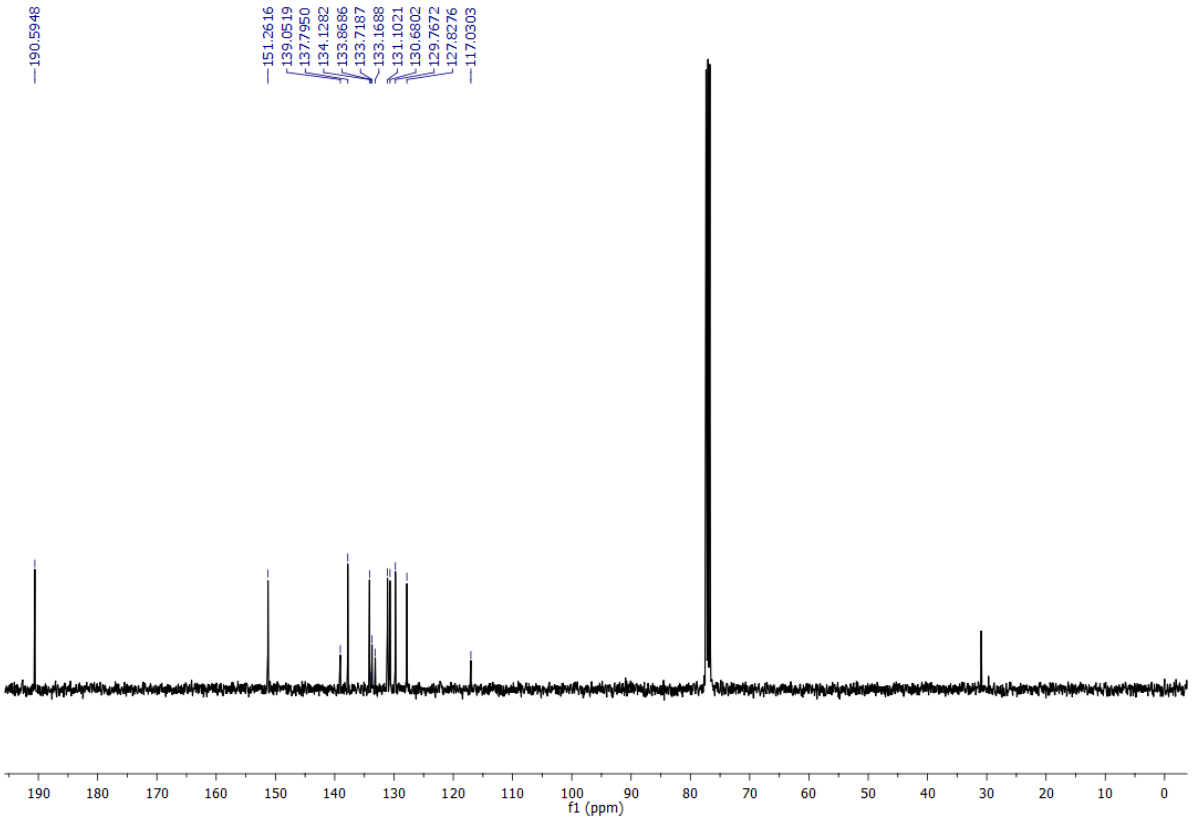

Fig. S22 ^{13}C NMR spectra of 5-(2-formylphenyl)picolinonitrile

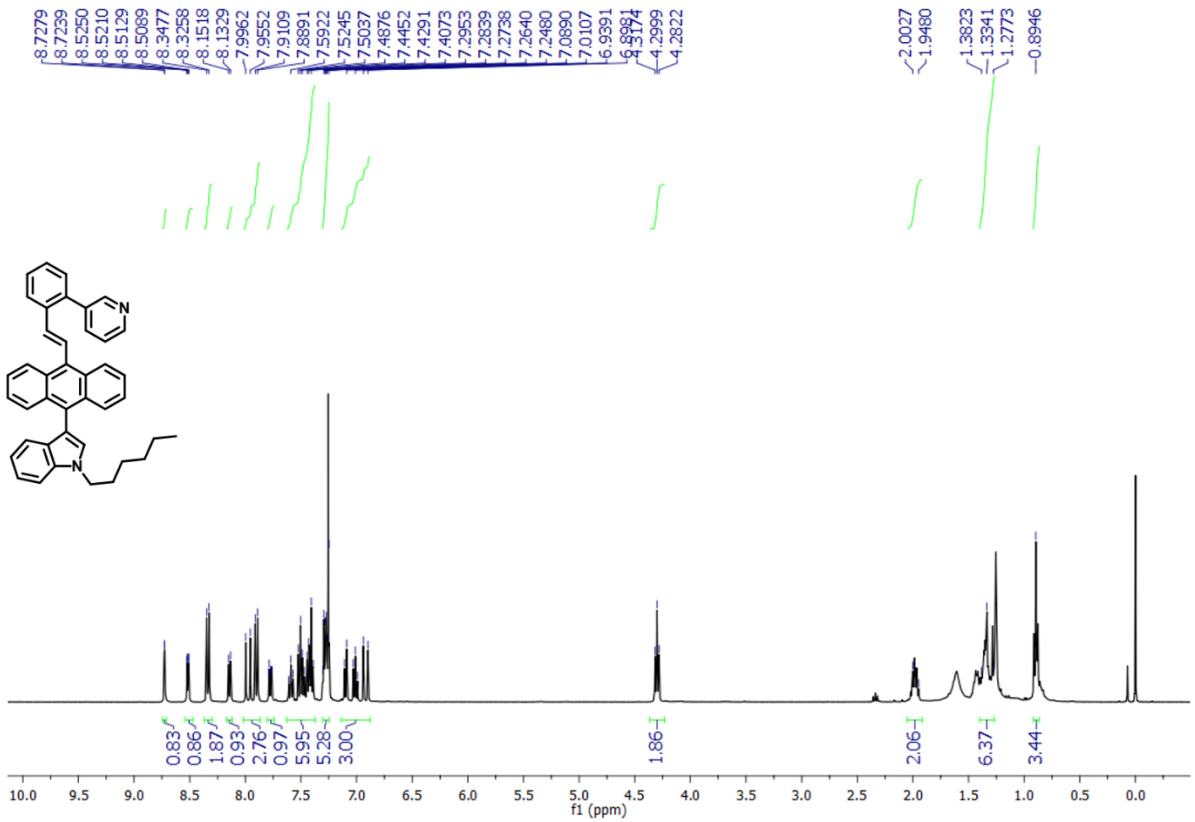

Fig. S23 ^{1}H NMR spectra of (E)-1-hexyl-3-(10-(2-(pyridin-3-yl)styryl)anthracen-9-yl)-1H-indole

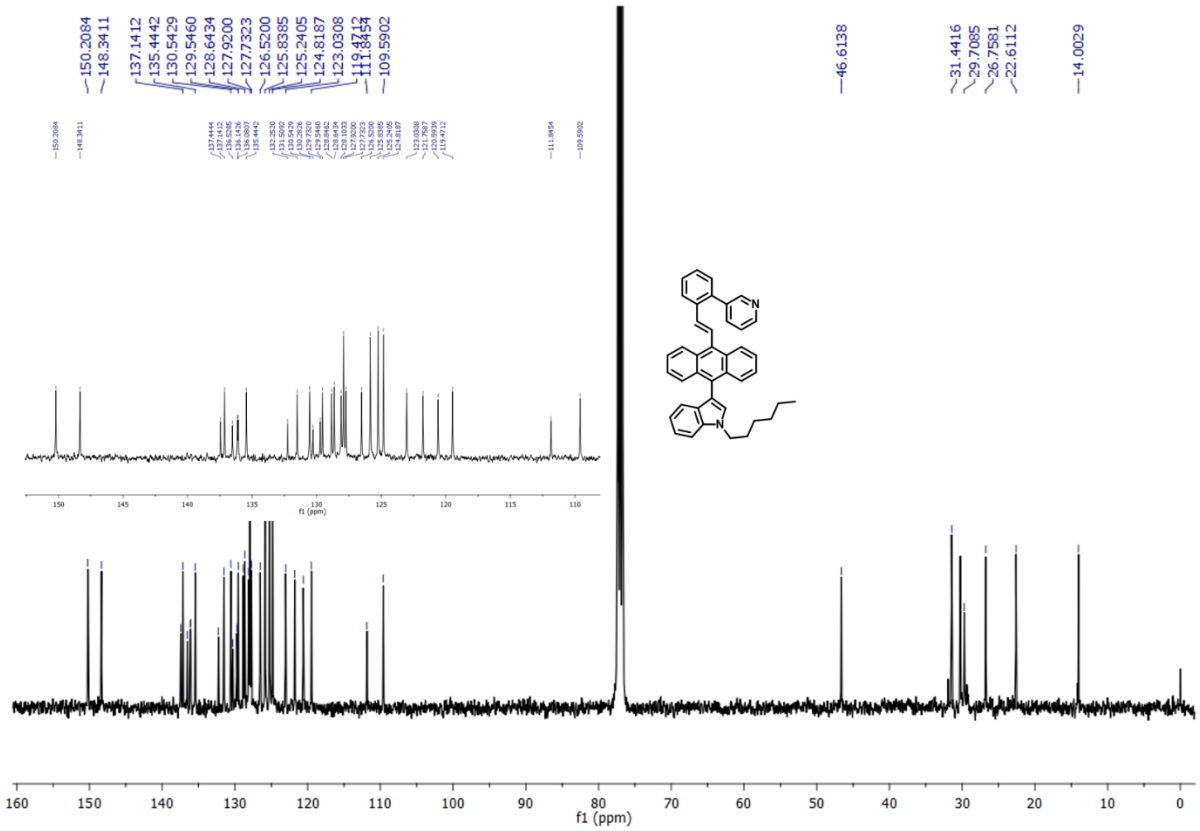

Fig. S24 ^{13}C NMR spectra of (E)-1-hexyl-3-(10-(2-(pyridin-3-yl)styryl)anthracen-9-yl)-1H-indole

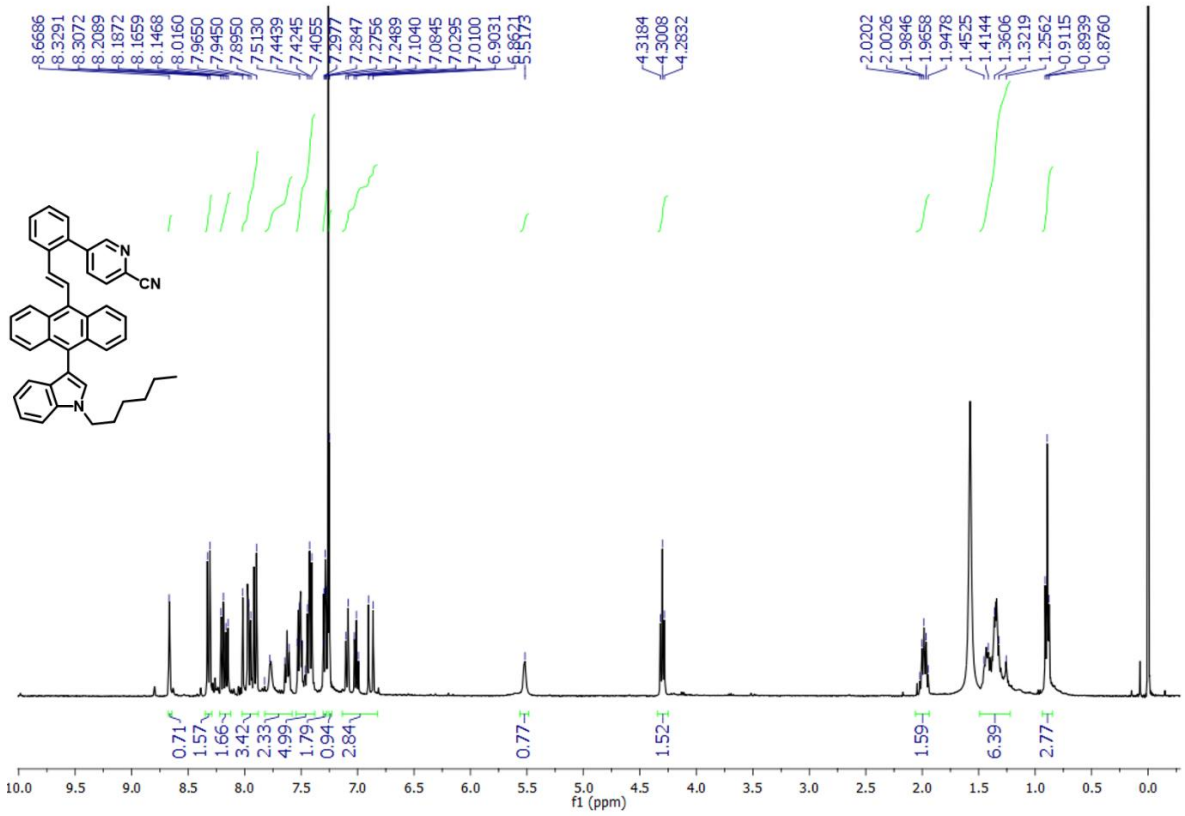

Fig. S25 ^{1}H NMR spectra of (E)-5-(2-(2-(10-(1-hexyl-1H-indol-3-yl)anthracen-9-yl)vinyl)phenyl)picolinonitrile

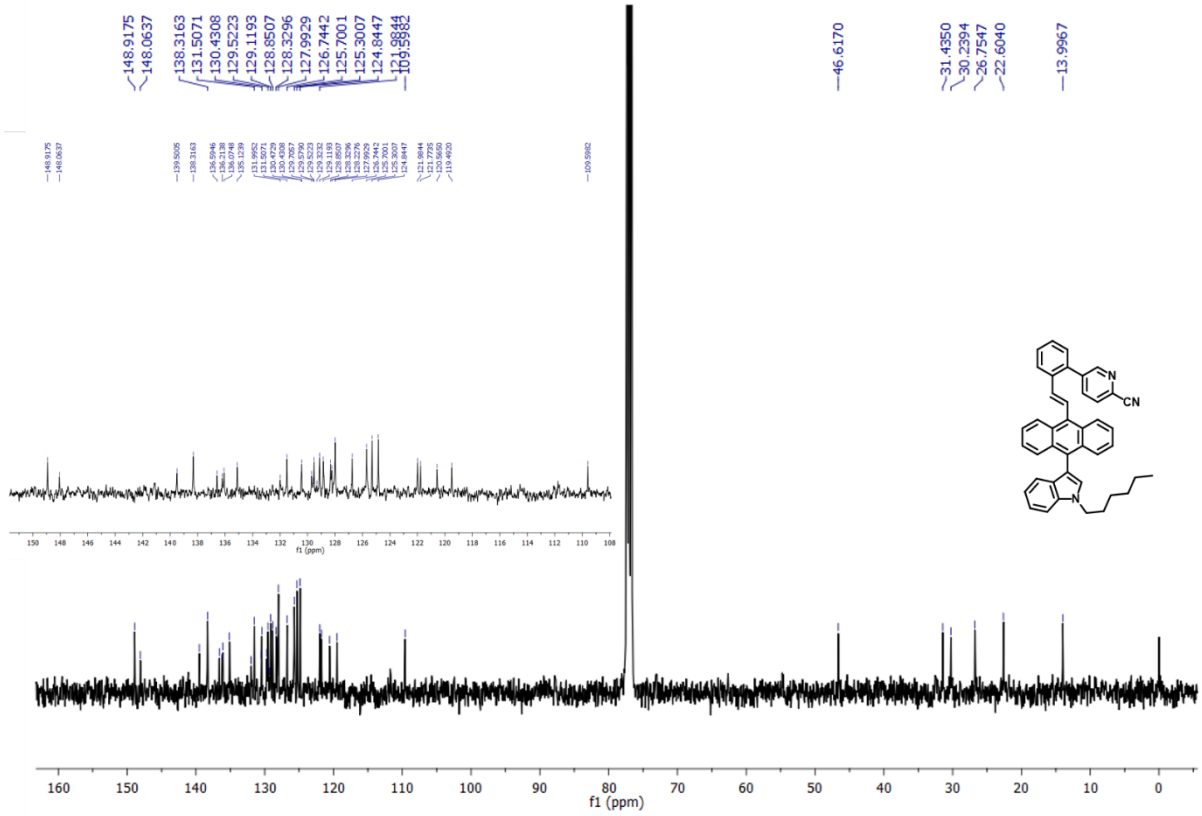

Fig. S26 ^{13}C NMR spectra of (E)-5-(2-(2-(10-(1-hexyl-1H-indol-3-yl)anthracen-9-yl)vinyl)phenyl)picolinonitrile

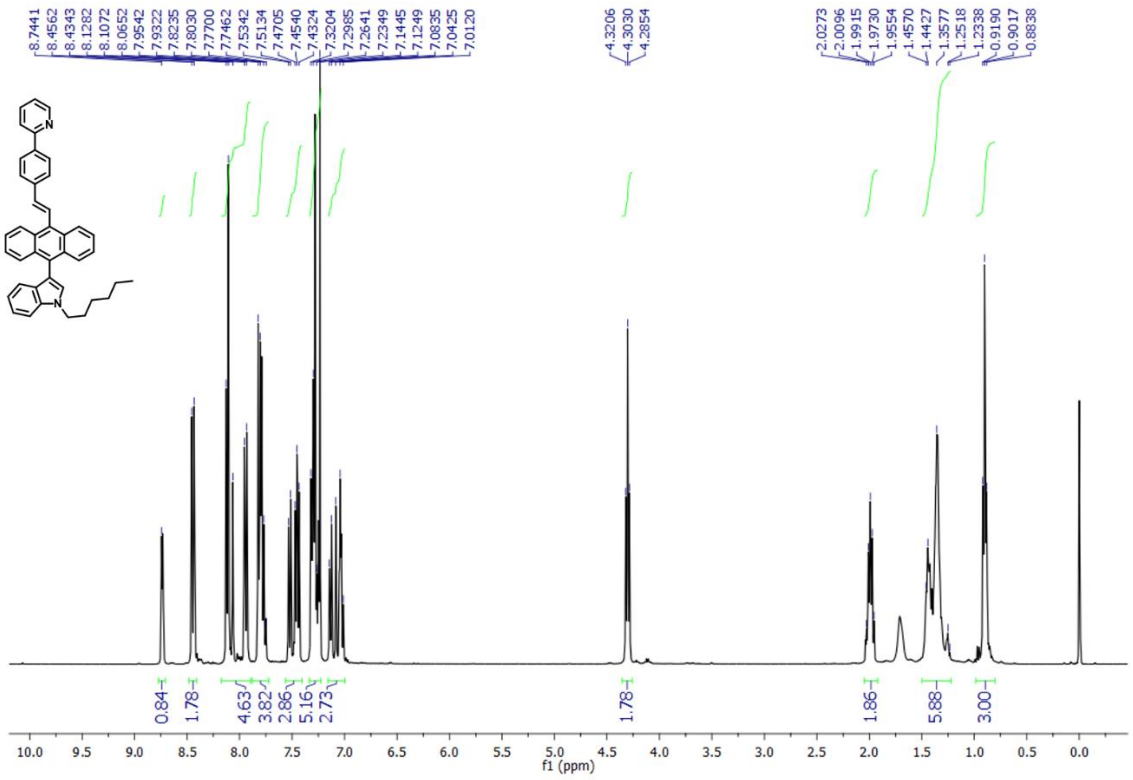

Fig. S27 ^{1}H NMR spectra of (E)-1-hexyl-3-(10-(4-(pyridin-2-yl)styryl)anthracen-9-yl)-1H-indole

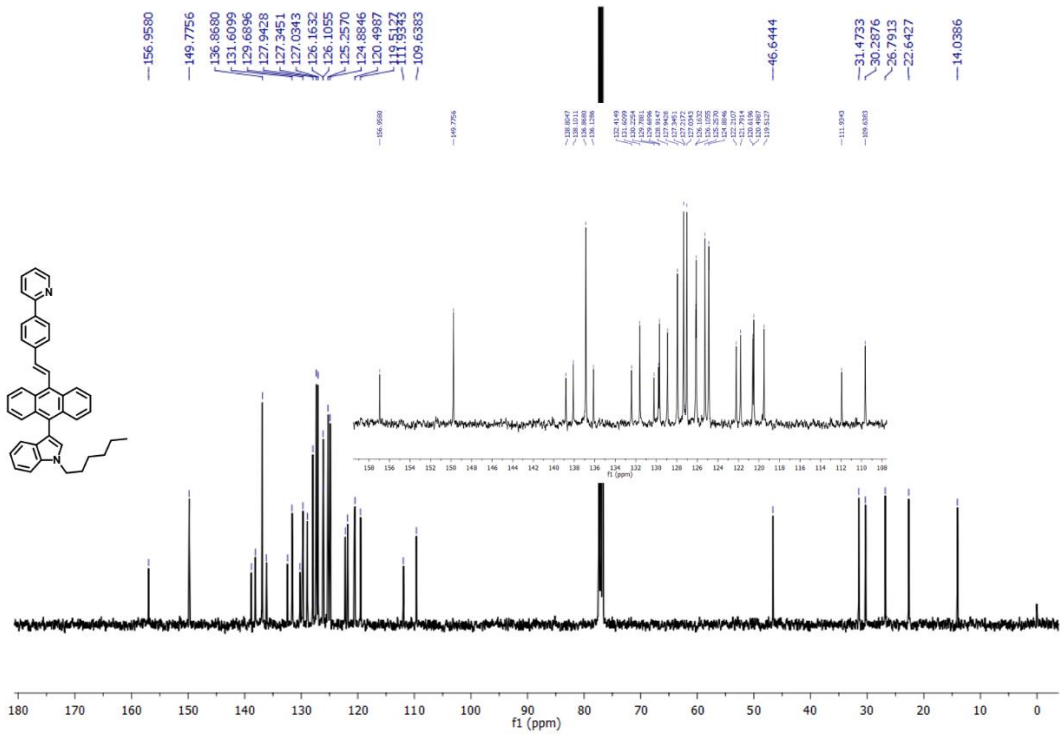

Fig. S28 ^{13}C NMR spectra of (E)-1-hexyl-3-(10-(4-(pyridin-2-yl)styryl)anthracen-9-yl)-1H-indole

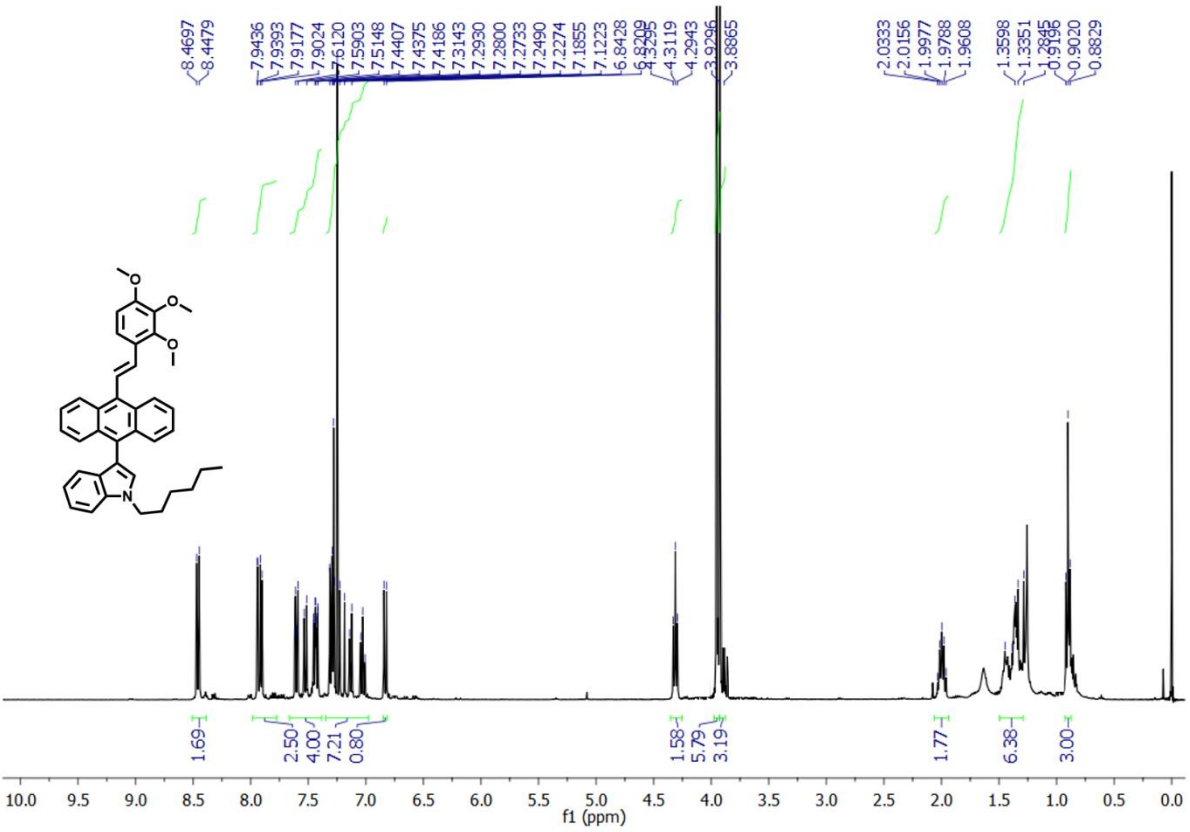

Fig. S29 ^{1}H NMR spectra of (E)-1-hexyl-3-(10-(2,3,4-trimethoxystyryl)anthracen-9-yl)-1H-indole

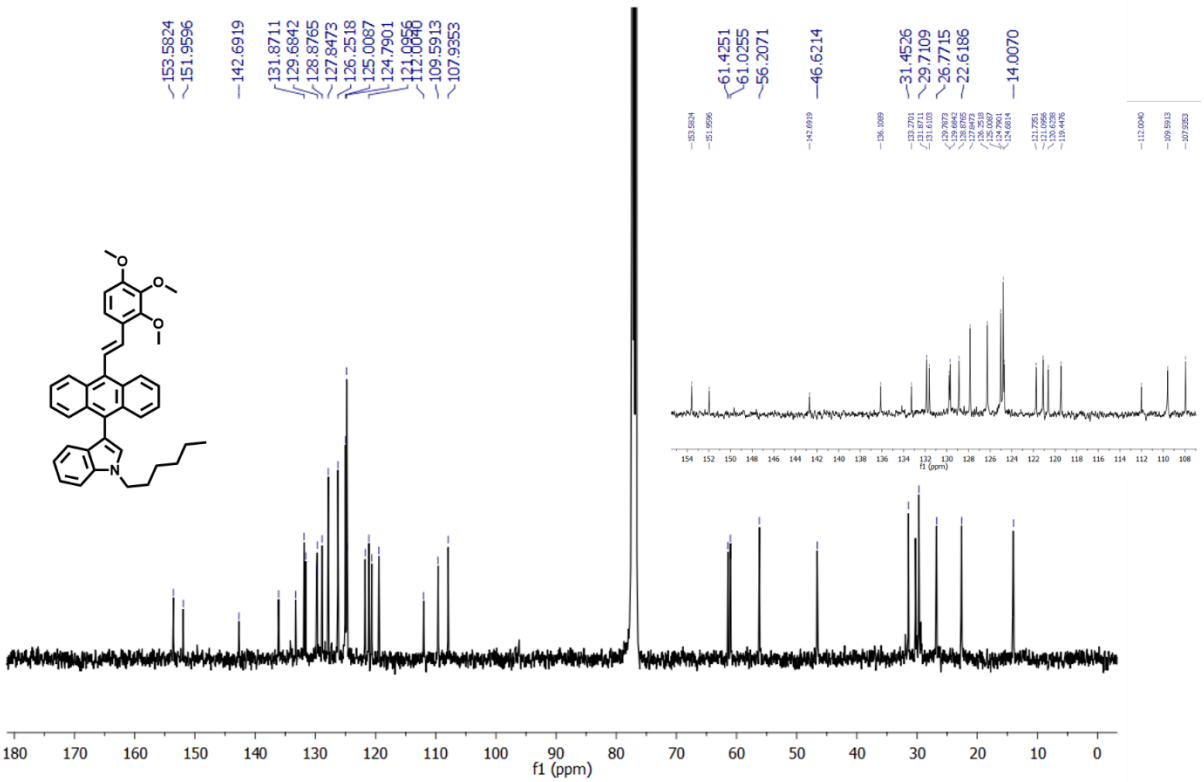

Fig. S30 ^{13}C NMR spectra of (E)-1-hexyl-3-(10-(2,3,4-trimethoxystyryl)anthracen-9-yl)-1H-indole

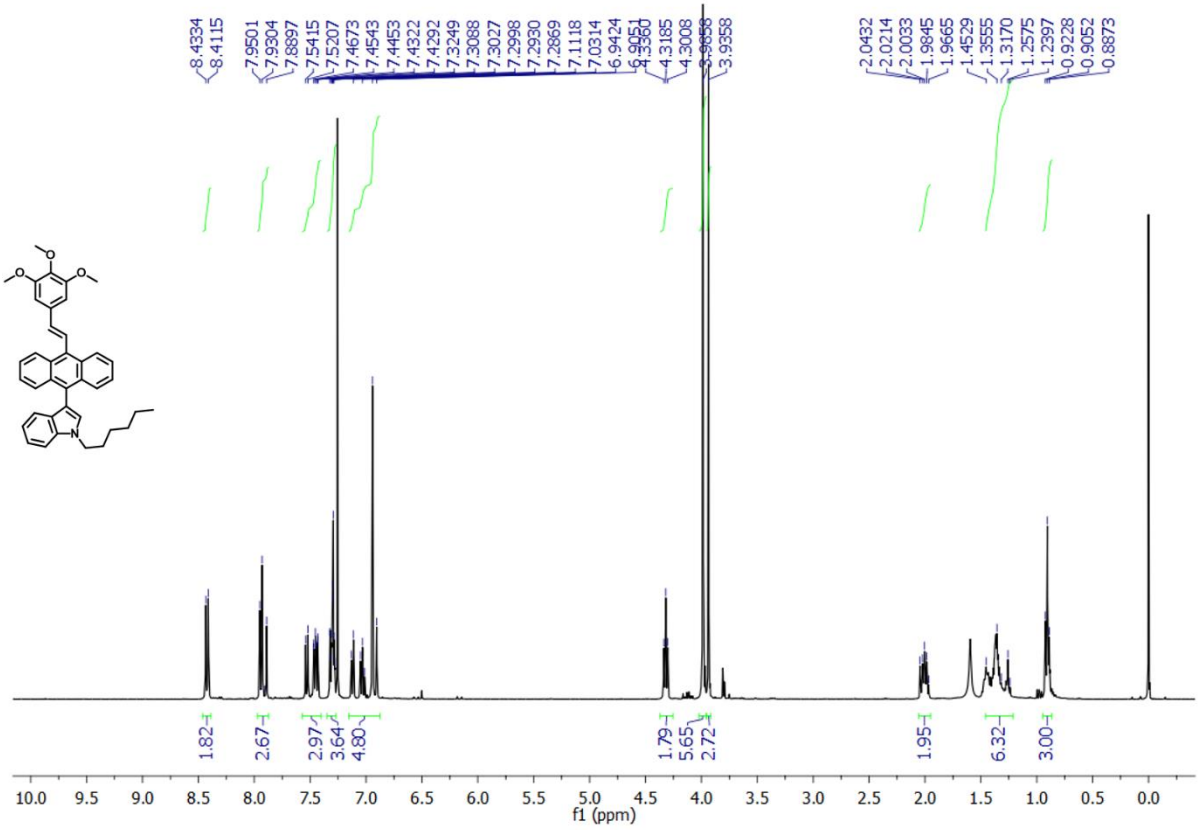

Fig. S31 ^{1}H NMR spectra of (E)-1-hexyl-3-(10-(3,4,5-trimethoxystyryl)anthracen-9-yl)-1H-indole

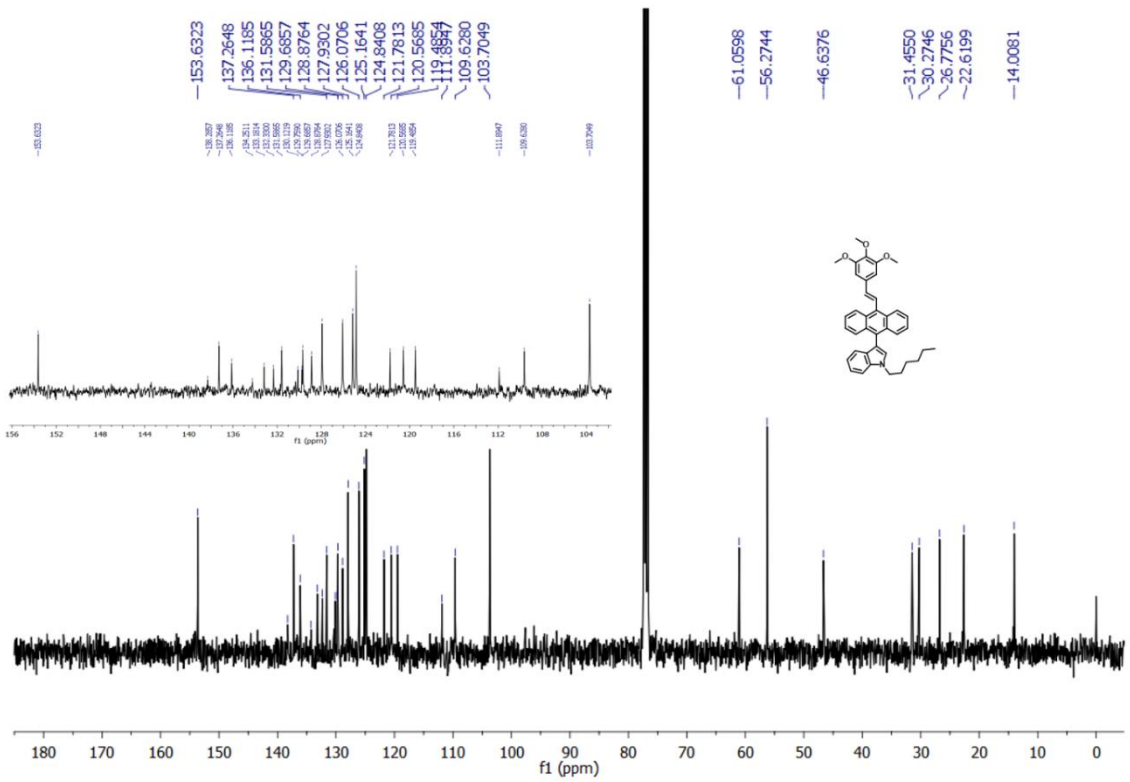

Fig. S32 ^{13}C NMR spectra of (E)-1-hexyl-3-(10-(3,4,5-trimethoxystyryl)anthracen-9-yl)-1H-indole

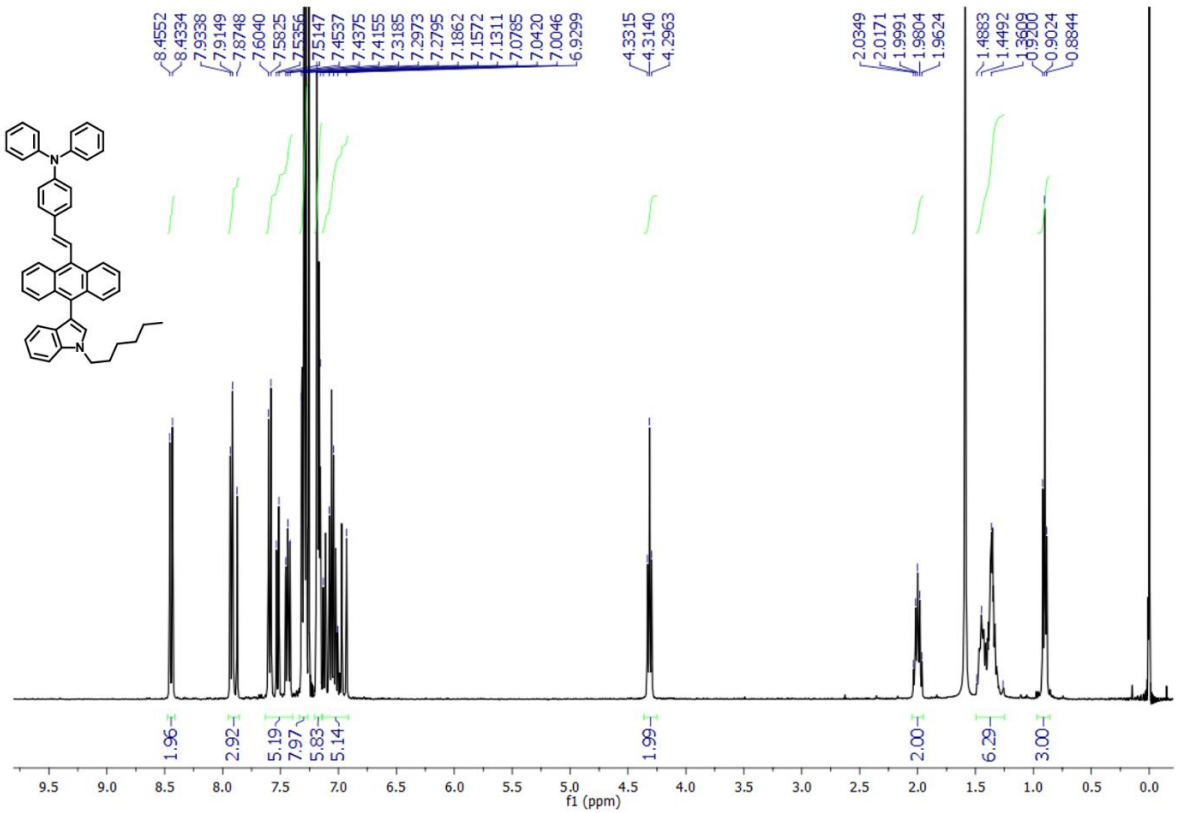

Fig. S33 ^{1}H NMR spectra of (E)-4-(2-(10-(1-hexyl-1H-indol-3-yl)anthracen-9-yl)vinyl)-N,N-diphenylaniline

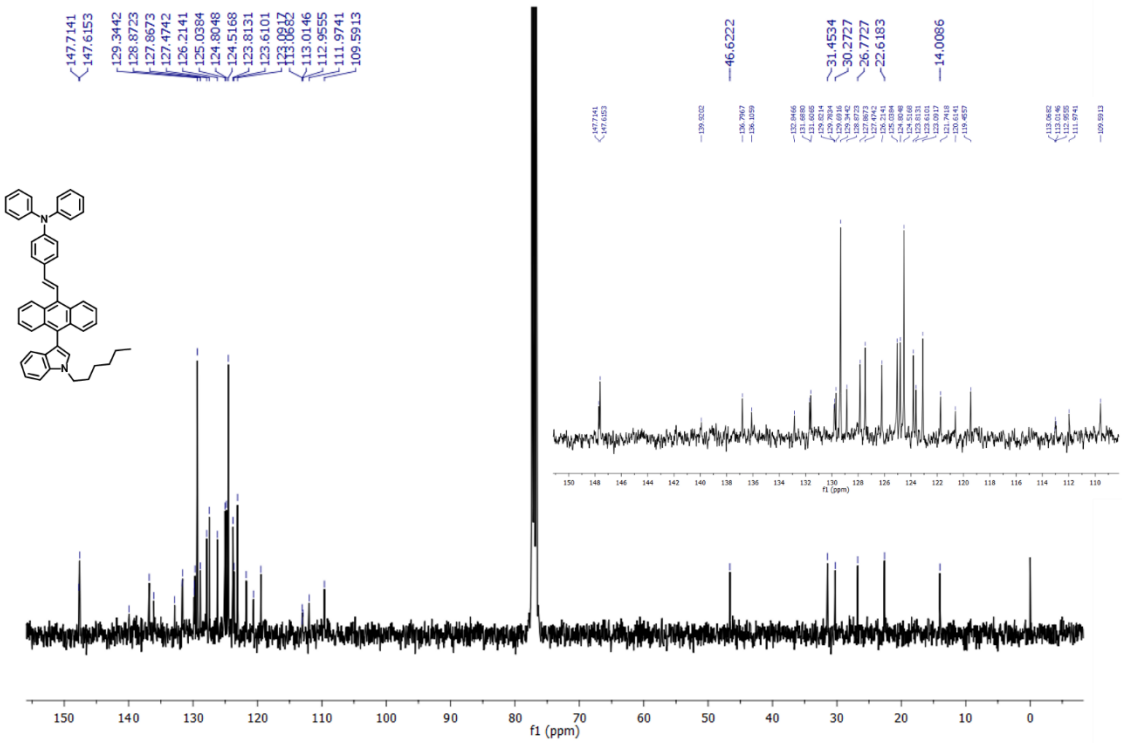

Fig. S34 ^{13}C NMR spectra of (E)-4-(2-(10-(1-hexyl-1H-indol-3-yl)anthracen-9-yl)vinyl)-N,N-diphenylaniline

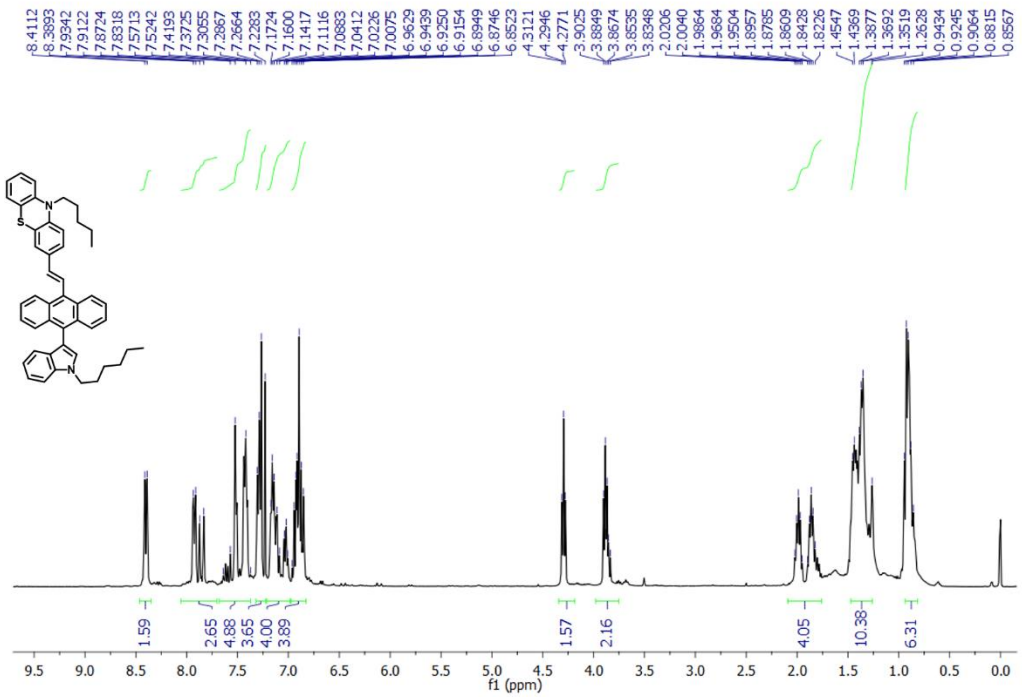

Fig. S35 ^{1}H NMR spectra of (E)-3-(2-(10-(1-hexyl-1H-indol-3-yl)anthracen-9-yl)vinyl)-10-pentyl-10H-phenothiazine

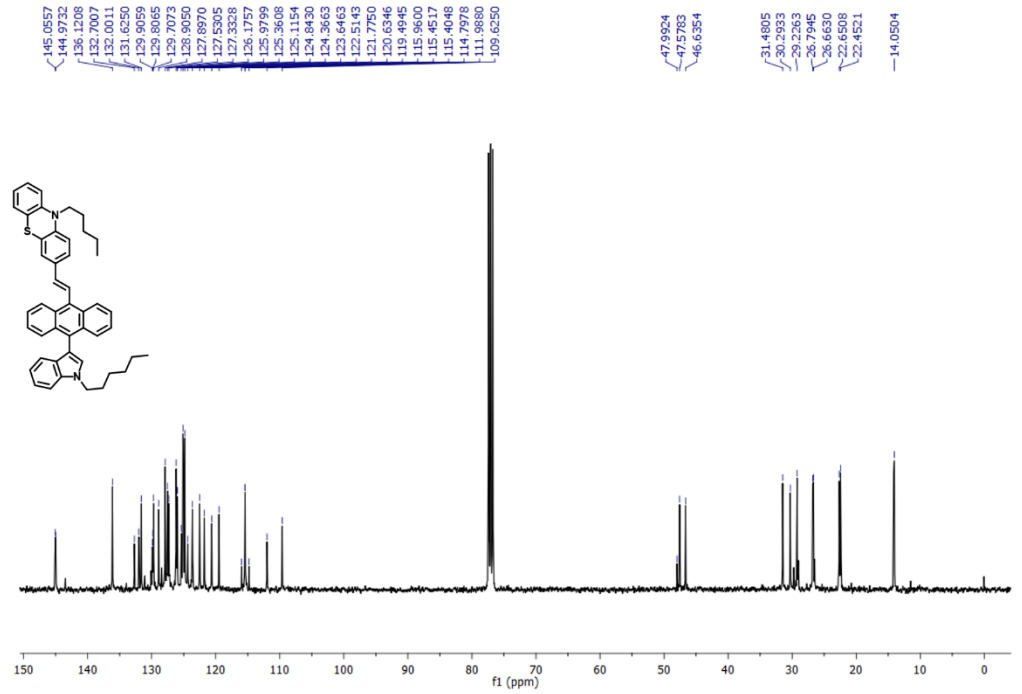

Fig. S36 ^{13}C NMR spectra of of (E)-3-(2-(10-(1-hexyl-1H-indol-3-yl)anthracen-9-yl)vinyl)-10-pentyl-10H-phenothiazine

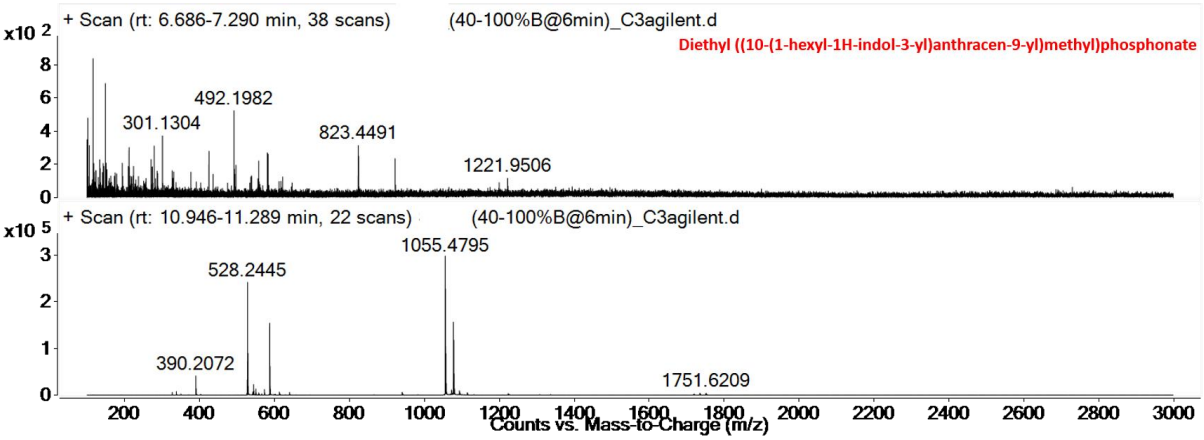
+ Scan (rt: 6.686-7.290 min, 38 scans) (40-100%B@6min)_C3agilent.d
Diethyl ((10-(1-hexyl-1H-indol-3-yl)anthracen-9-yl)methyl)phosphonate
x10 2
492.1982
301.1304
823.4491
1221.9506
+ Scan (rt: 10.946-11.289 min, 22 scans) (40-100%B@6min)_C3agilent.d
x10 5
1055.4795
528.2445
390.2072
1751.6209
Counts vs. Mass-to-Charge (m/z)

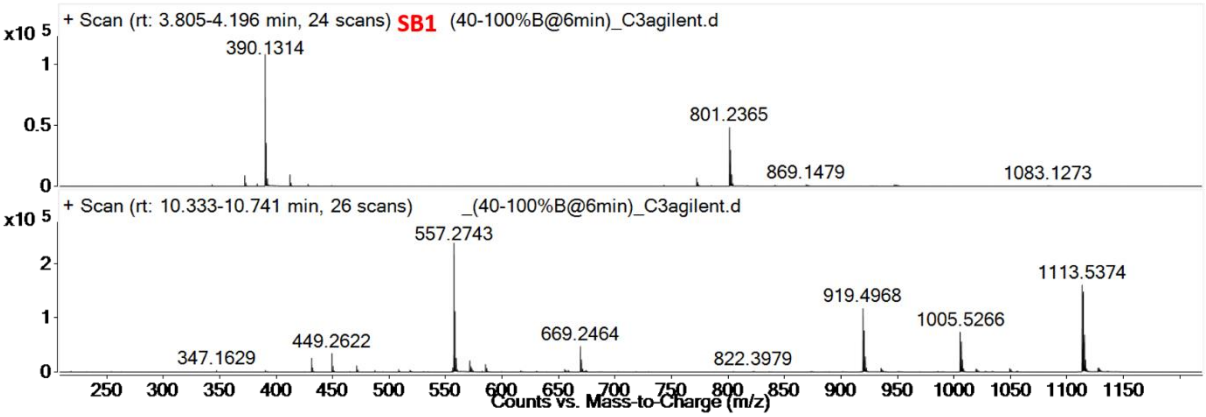
+ Scan (rt: 3.805-4.196 min, 24 scans) SB1 (40-100%B@6min)_C3agilent.d
x10 5
390.1314
801.2365
869.1479
1083.1273
+ Scan (rt: 10.333-10.741 min, 26 scans) _(40-100%B@6min)_C3agilent.d
557.2743
1113.5374
919.4968
1005.5266
669.2464
449.2622
347.1629
822.3979
Counts vs. Mass-to-Charge (m/z)

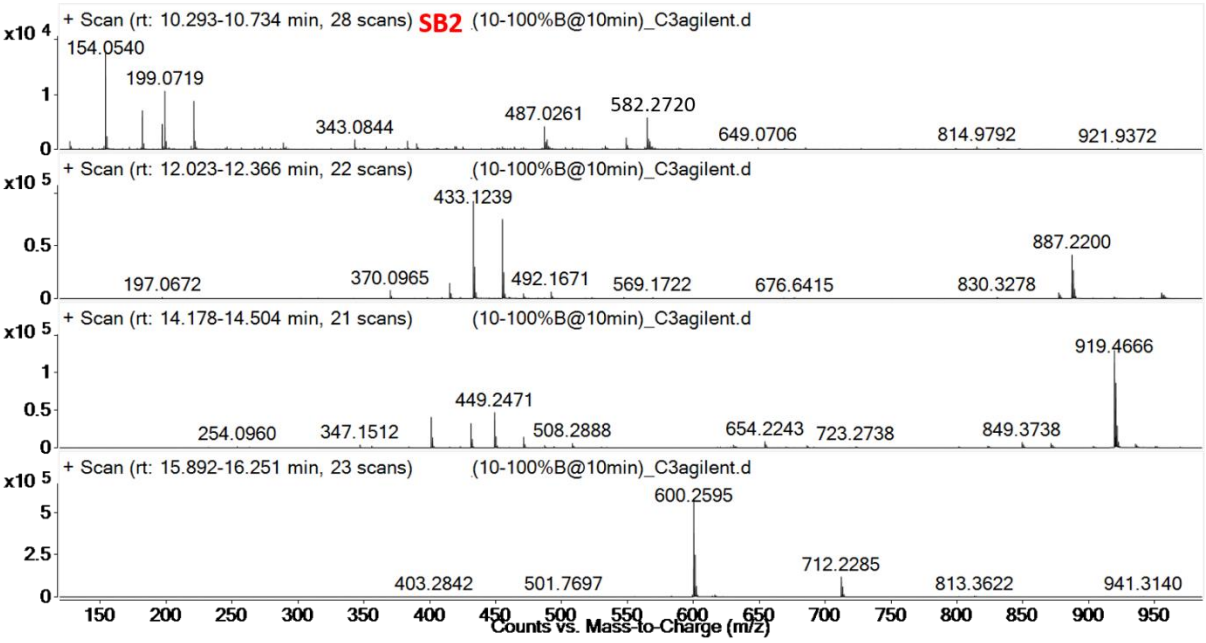
+ Scan (rt: 10.293-10.734 min, 28 scans) SB2 (10-100%B@10min)_C3agilent.d
x10 4
154.0540
199.0719
343.0844
487.0261
582.2720
649.0706
814.9792
921.9372
+ Scan (rt: 12.023-12.366 min, 22 scans) (10-100%B@10min)_C3agilent.d
x10 5
433.1239
887.2200
197.0672
370.0965
492.1671
569.1722
676.6415
830.3278
+ Scan (rt: 14.178-14.504 min, 21 scans) (10-100%B@10min)_C3agilent.d
x10 5
919.4666
449.2471
254.0960
347.1512
508.2888
654.2243
723.2738
849.3738
+ Scan (rt: 15.892-16.251 min, 23 scans) (10-100%B@10min)_C3agilent.d
x10 5
600.2595
712.2285
403.2842
501.7697
813.3622
941.3140
Counts vs. Mass-to-Charge (m/z)

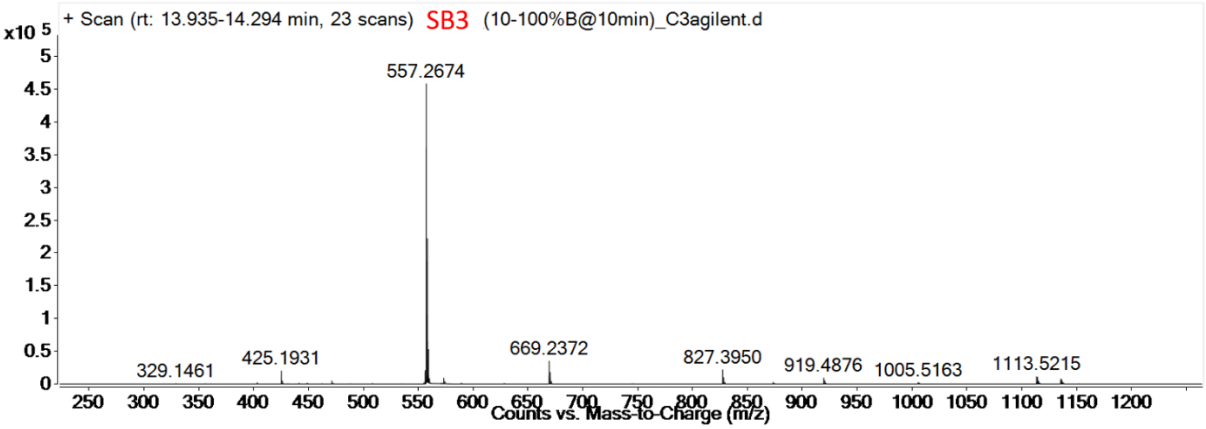
+ Scan (rt: 13.935-14.294 min, 23 scans) SB3 (10-100%B@10min)_C3agilent.d
x10 5
557.2674
329.1461
425.1931
669.2372
827.3950
919.4876
1005.5163
1113.5215
Counts vs. Mass-to-Charge (m/z)

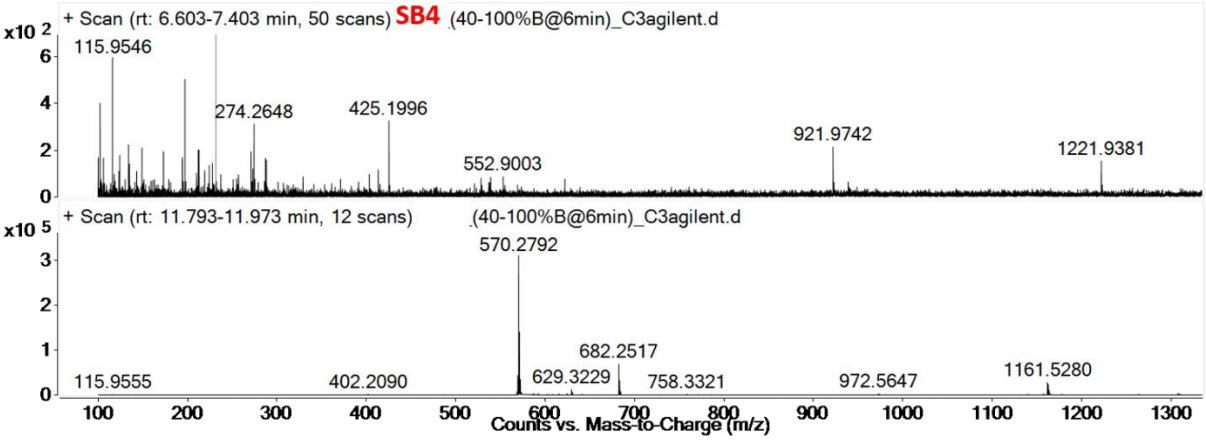
+ Scan (rt: 6.603-7.403 min, 50 scans) SB4 (40-100%B@6min)_C3agilent.d
x10 2
115.9546
274.2648
425.1996
552.9003
921.9742
1221.9381
+ Scan (rt: 11.793-11.973 min, 12 scans) (40-100%B@6min)_C3agilent.d
x10 5
570.2792
682.2517
115.9555
402.2090
629.3229
758.3321
972.5647
1161.5280
Counts vs. Mass-to-Charge (m/z)

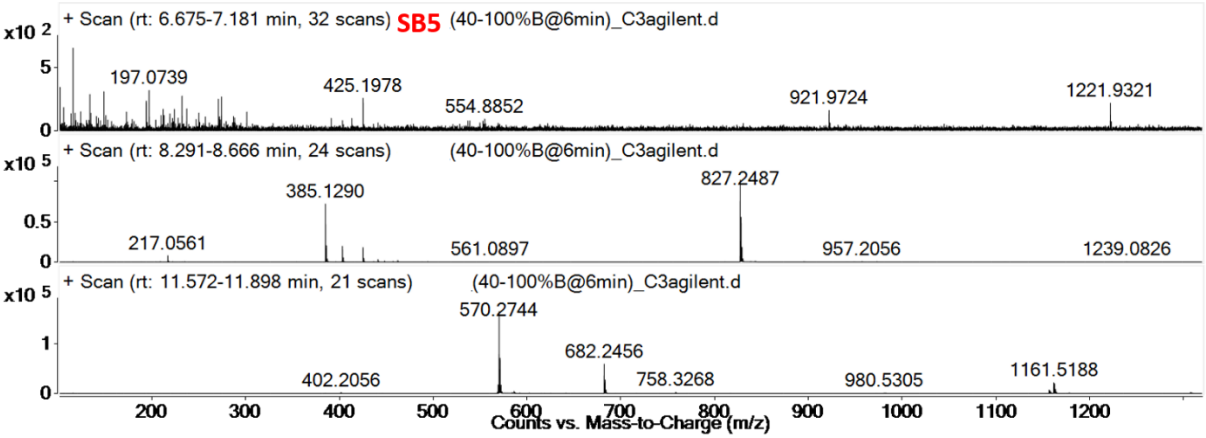
+ Scan (rt: 6.675-7.181 min, 32 scans) SB5 (40-100%B@6min)_C3agilent.d
x10 2
197.0739
425.1978
554.8852
921.9724
1221.9321
+ Scan (rt: 8.291-8.666 min, 24 scans) (40-100%B@6min)_C3agilent.d
x10 5
385.1290
827.2487
217.0561
561.0897
957.2056
1239.0826
+ Scan (rt: 11.572-11.898 min, 21 scans) (40-100%B@6min)_C3agilent.d
x10 5
570.2744
682.2456
402.2056
758.3268
980.5305
1161.5188
Counts vs. Mass-to-Charge (m/z)

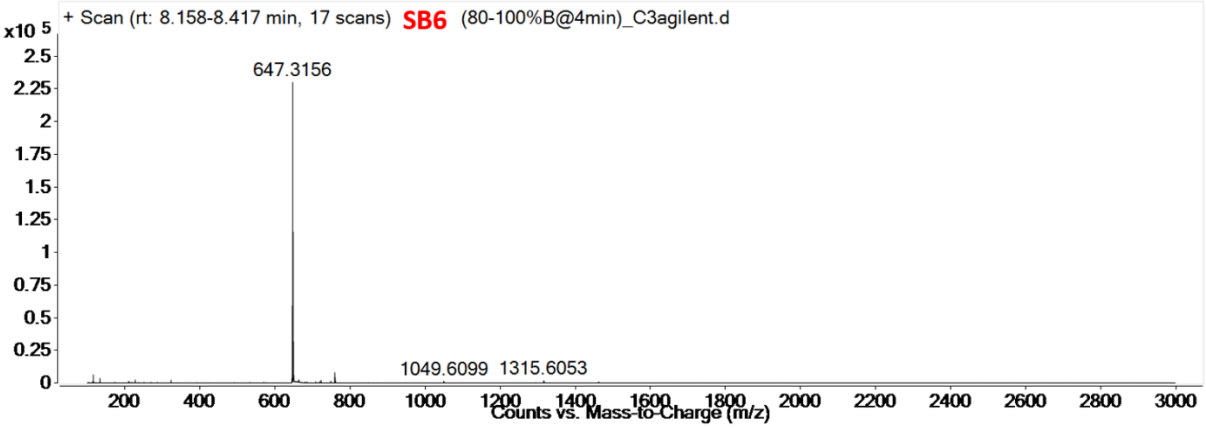
+ Scan (rt: 8.158-8.417 min, 17 scans) SB6 (80-100%B@4min)_C3agilent.d
x10 5
647.3156
1049.6099
1315.6053
Counts vs. Mass-to-Charge (m/z)

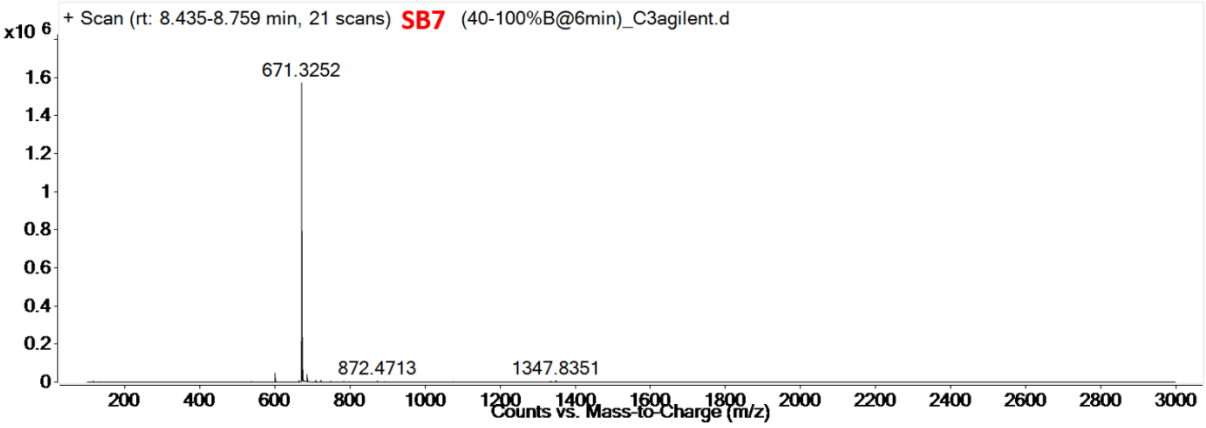

Fig. S37 HR-MS spectra of the synthesized compounds

References:

1. Neese, F.; Wennmohs, F.; Becker, U.; Riplinger, C. “The ORCA Quantum Chemistry Program Package.” *Journal of Chemical Physics*, 2020, **152**, 224108.

2. Neese, F. “Software Update: The ORCA Program System-Version 5.0.”*WIREs Computational Molecular* Science, 2022**, 2**, 73-78.

3. T. Yanai, D. Tew, and N. Handy, “A new hybrid exchange-correlation functional using the Coulomb-attenuating method (CAM-B3LYP),”*Chem. Phys. Lett.*, 2004**, 393**, 51-57.

4. Kabsch W., A solution for the best rotation to relate two sets of vectors, *Acta Crystallogr.,* 1976, **A32**, 922-923. (Code: https://github.com/charnley/rmsd)

5. Hanwell, Marcus D., et al. "Avogadro: an advanced semantic chemical editor, visualization, and analysis platform."*J. Cheminformatics*, 2012, **4**, 1-17.